Chapter II

THEORETICAL BACKGROUND AND EXPERIMENTAL TECHNIQUES

THEORIES OF LIQUID CRYSTALLINE PHASES

The theories of liquid crystalline phases have been described at length in several books [1-5]. Only the salient features of the mean field theories of nematic and smectic A phases developed respectively by Maier-Saupe [6] and McMillan [7,8] have been discussed here since some of the experimental results presented in this dissertation have been compared with these theories.

The molecular field theory has been extremely useful in developing the spontaneous long range orientational order and other related properties of nematic phase. Considering the medium as an assembly of permanent electric dipoles, M. Born in 1916 proposed the first molecular field theory of the nematic phase [9]. However, it is now known that the molecules forming the liquid crystalline phases need not possess permanent dipole moment as a pre-requisite.

The theory developed by Maier-Saupe (MS), based on the molecular field approximations, explains effectively the nematic isotropic (N-I) transition in terms of the orientational order parameters. On the basis of Landau theory of phase transitions [10] de Gennes proposed a phenomenological description on the existence of nematic like short-range order in isotropic phase [11]. The first molecular statistical treatment of the smectic nematic (Sm-N) transition was given by Kobayashi [12,13] by including an additional isotropic intermolecular interaction in MS model. A simple but elegant description of the SmA phase was given by McMillan [7,8] in which he included additional translational order parameter characterizing the layered structure and assuming that the director is normal to the layers. In the Kobayashi-McMillan approach an ad hoc orientational interaction is also introduced, however the effects of short range order and fluctuation of the order parameters are neglected [7,8]. The details of the McMillan, Wulf and de Gennes theories on SmC liquid crystals and the Meyer-McMillan theory on of SmC, -B, and –H liquid crystals are given in reference [14,15].

Computer simulation techniques are also extremely used to study the liquid crystalline phases by adopting several models viz., soft, hard and realistic

models involving atom-atom potentials and using monte-carlo or molecular dynamics method [16-24].

Maier-Saupe Mean field theory of the nematic phase

The MS theory is based on the idea that the existence of nematic phase is due to the anisotropic part of the dispersion forces between the molecules. It is assumed that each molecule is subjected to an average internal field that is independent of any local variations or short-range ordering. The exact nature of the intermolecular forces need not be known. The nematic phase is assumed to be composed off rod-like molecules in which (i) the molecules are cylindrically symmetric about the axis of preferred orientations **n** and (ii) the directions **n** and – **n** are fully equivalent i.e. preferred axis is non-polar.

The degree of alignment of the molecules with respect to the director **n** is described by an orientational order parameter given by

$$S = \langle P_2(\cos\beta_i)\rangle = \frac{1}{2}\langle 3\cos^2\beta_i - 1\rangle \qquad (2.1)$$

where β_i is the angle between the long axis of the $\mathbf{i}^{th}$ molecule and the director **n** and $P_2(\cos\beta_i)$ is the second order Legendre polynomial. Here $\langle ... \rangle$ denotes statistical average over all β_i.

The orientational energy of the i^{th} molecule is given by [25]:

$$u_i(\cos\beta_i) \propto -\langle P_2(\cos\beta_i)\rangle P_2(\cos\beta_i)$$

so that,

$$u_i(\cos\beta_i) = -v\langle P_2(\cos\beta_i)\rangle P_2(\cos\beta_i)$$

i.e.,

$$u_i(\cos\beta_i) = -\frac{A}{V^2}\langle P_2(\cos\beta_i)\rangle P_2(\cos\beta_i) \qquad (2.2)$$

where V is the molar volume of the sample and A is taken to be a constant independent of pressure, volume and temperature. Also, $v = \frac{A}{V^2}$ is the coupling constant.

Humphries, James and Luckhurst [26] developed a more comprehensive concept by including higher order terms in the mean field potential for cylindrically symmetric molecules. Thus u_i was taken as

$$u_i(\cos\beta_i) = \sum_{L\,even} u_{Li} \langle P_L(\cos\beta_i)\rangle P_L(\cos\beta_i) \qquad (L\neq 0)$$

where $P_L(\cos\beta_i)$ is the L^{th} order Legendre polynomial.

Orientational Distribution Function and the Order Parameters

As the potential energy of each molecule is known, the fact that the system must be in thermodynamic equilibrium demands that the probability of a molecule being oriented at an angle β_i from the director is given by the Boltzmann factor, therefore the orientational distribution function for the molecules is

$$f(\cos\beta_i) = Z^{-1} \exp\left[\frac{-u_i(\cos\beta_i)}{kT}\right]$$

where k is the Boltzmann constant, T is temperature in absolute scale and Z being the partition function for a single molecule. Z is given by

$$Z = \int_0^1 \exp\left[\frac{-u(\cos\beta)}{kT}\right] d(\cos\beta)$$

for brevity we drop the subscript i.

The order parameter, S, is therefore written as

$$S = \langle P_2\rangle = \int_0^1 P_2(\cos\beta) f(\cos\beta) d(\cos\beta)$$

$$= \frac{\int_0^1 P_2(\cos\beta)\exp[v\langle P_2\rangle P_2(\cos\beta)/kT]d(\cos\beta)}{\int_0^1 \exp[v\langle P_2\rangle P_2(\cos\beta)/kT]d(\cos\beta)}$$

$$\text{i.e., } \langle P_2\rangle = \frac{\int_0^1 P_2(\cos\beta)\exp[\langle P_2\rangle P_2(\cos\beta)/T^*]d(\cos\beta)}{\int_0^1 \exp[\langle P_2\rangle P_2(\cos\beta)/T^*]d(\cos\beta)} \qquad (2.3)$$

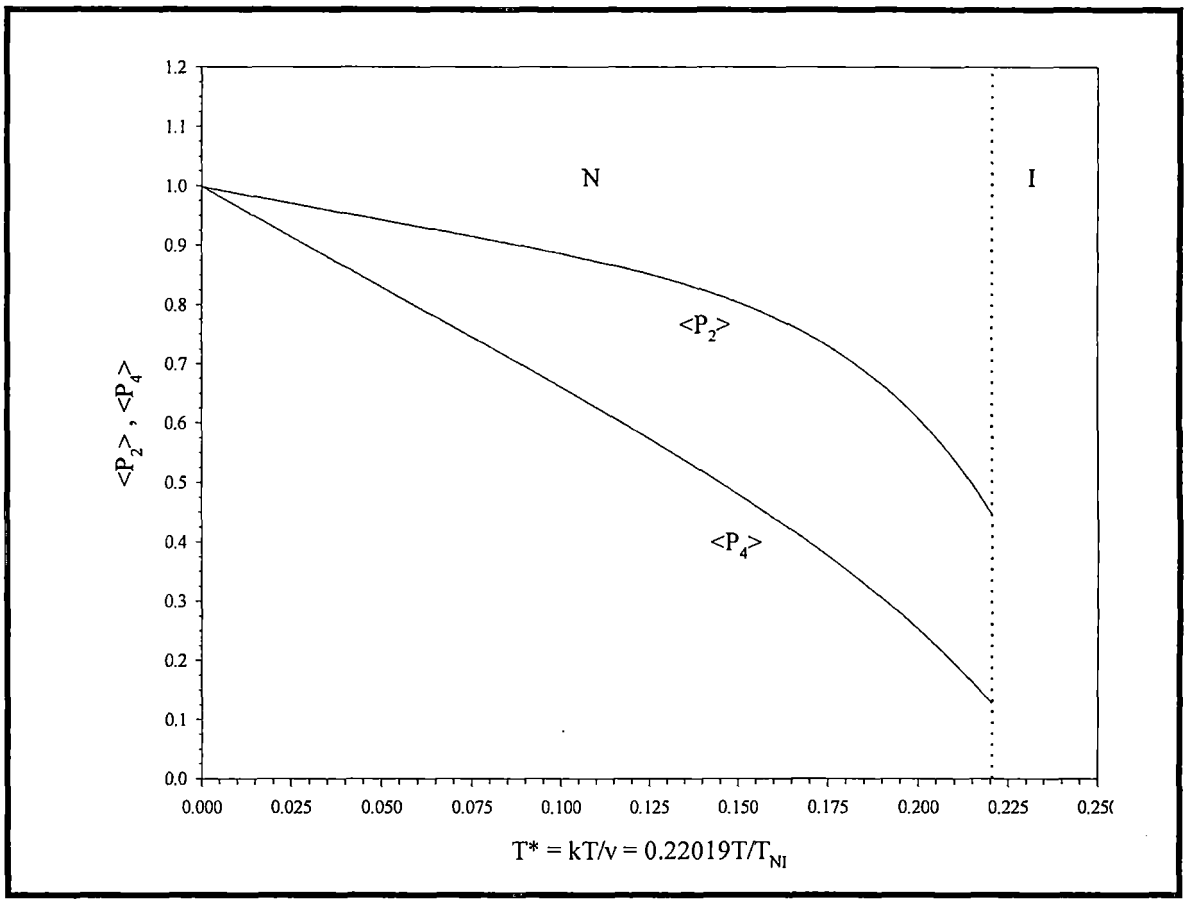

Figure 2.1 Order parameters $\langle P_2 \rangle$ and $\langle P_4 \rangle$ versus reduced temperature predicted from MS theory.

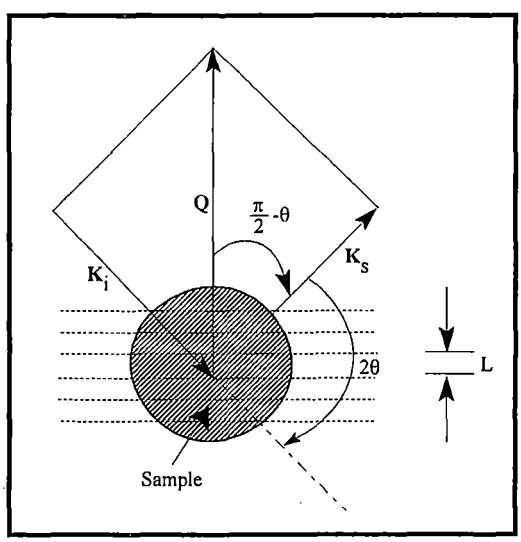

Figure 2.2 Typical scattering geometry showing the incident ($\mathbf{K}_i$), scattered ($\mathbf{K}_s$) and scattering ($\mathbf{Q}$) wave vectors. L is layer spacing.

where T* = kT/v is called the reduced temperature.

Equation (2.3) contains $<P_2>$ on both sides, a self-consistent equation for the determination of the temperature dependence of $<P_2>$. For all values of T*, it is observed that $<P_2> = 0$ is a solution, showing a disordered phase, i.e. the normal isotropic liquid. For $T^* < 0.22284$ two more solutions of $<P_2>$ appear. A state with positive $<P_2>$ which tends to unity at $T^* = 0$ can be identified with nematic phase. Other is one with negative $<P_2>$, corresponds to an unstable phase. The laws of thermodynamics demands, the state with minimum free energy is the stable one. Applying this condition, we get the region $0 \leq T^* \leq 0.22019$ where $\langle P_2 \rangle$ is greater than zero corresponding to the anisotropic nematic phase and for $T^* > 0.22019$, the isotropic phase with $\langle P_2 \rangle = 0$.

According to the Maier-Saupe theory, the nematic-isotropic liquid transition occurs at $T^* = 0.22019$ and $\langle P_2 \rangle = 0.4289$. Thus the N-I transition is first order and for many liquid crystals the $\langle P_2 \rangle$ values obtained from Maier-Saupe theory agrees quite well with the observed experimental values.

The higher order parameter $\langle P_4 \rangle$ can be obtained using the 4th order Legendre polynomial which is,

$$\langle P_4(\cos\beta) \rangle = \frac{1}{8}(35\langle \cos^4 \beta \rangle - 30\langle \cos^2 \beta \rangle + 3) \qquad (2.4)$$

The temperature dependence of $\langle P_2 \rangle$ and $\langle P_4 \rangle$ is shown in **Figure 2.1**. The nature of temperature variation of $\langle P_4 \rangle$ also indicates 1st order N-I transition. Moreover, temperature dependence of the order parameters is universal in character, there are no parameters that can be adjusted to allow for different order parameter behaviour of different compounds.

Humphries, James and Luckhurst [27] and later by Palffy-Muhoray et al.[28], extended the MS theory to investigate the properties of binary mixtures. The latter treatment has led to some important conclusions [29]:

(i) There can be a nematic-nematic coexisting region, for certain values of the parameters. The coexisting nematic phase has been observed in

mixtures of polymeric, low molecular mass nematogens, both with rod-shaped and disc-shaped molecules.

(ii) The order parameters of the mixture and its variation with temperature agree very closely with the Maier-Saupe universal curve. However, the order parameters of the pure components of the mixture may differ appreciably. [30,31].

McMillan's Theory of Smectic A Phase

The MS mean-field model of nematics has been extended to describe the smectic A-nematic transition by several investigators [7,8,26-28]. By introducing an additional order parameter, in Maier-Saupe theory, to describe the one dimensional periodic layering of smectic phase, W.L. McMillan [7,8] could give a theory of smectic A..

Taking the periodic density variation along the layer normal to be the z-axis, besides the orientational distribution of the molecular axes, the normalized distribution function can be written as

$$f(z,\cos\beta) = \sum_{l\ \text{even}} \sum_{n} A_{l,n} P_l(\cos\beta)\cos\left(\frac{2\pi n z}{d}\right) \qquad (2.5)$$

with $$\int_{-1}^{1}\int_{0}^{d} f(z,\cos\beta)\,dz\,d(\cos\beta) = 1$$

as normalising condition, d being the layer thickness.

McMillan, following Kobayashi [12,13] form of potential, assumed a model potential of the following form

$$V_1(z,\cos\beta) = -v_0\left[\delta\alpha\tau\cos\left(\frac{2\pi z}{d}\right) + \left\{S + \sigma\alpha\cos\left(\frac{2\pi z}{d}\right)\right\}P_2(\cos\beta)\right] \qquad (2.6)$$

where, $S = \frac{1}{2}\langle 3\cos^2\beta - 1\rangle$ is the orientational order parameter,

$\tau = \langle \cos(\frac{2\pi z}{d}) \rangle$ is the translational order parameter, and

$\sigma = \langle P_2(\cos\beta)\cos(\frac{2\pi z}{d}) \rangle$ is the mixed order parameter,

and v_0 and δ are constants characterising respectively the strengths of the anisotropic and isotropic parts of the interaction, α is a parameter which depends on the core length and the molecular length. Obviously it reduces to MS potential when the two adjustable parameters δ and α become zero.

The distribution function in this case is

$$f_1(z,\cos\beta) = Z^{-1} \exp\left[-\frac{V_1(z,\cos\beta)}{kT}\right] \tag{2.7}$$

where the single molecular partition function Z is given by

$$Z = \int_0^d dz \int \exp\left[-\frac{V_1(z,\cos\beta)}{kT}\right] d(\cos\beta)$$

The various order parameters are, therefore, given by,

$$\left.\begin{aligned} S &= \int_0^d \int P_2(\cos\beta) f_1(z,\cos\beta)\, dz\, d(\cos\beta) \\ \tau &= \int_0^d \int \cos(\frac{2\pi z}{d}) f_1(z,\cos\beta)\, dz\, d(\cos\beta) \\ \sigma &= \int_0^d \int P_2(\cos\beta)\cos(\frac{2\pi z}{d}) f_1(z,\cos\beta)\, dz\, d(\cos\beta) \end{aligned}\right\} \tag{2.8}$$

These self-consistent equations can be solved numerically to find the temperature dependence of the three order parameters.

Out of several solutions, the equilibrium state is identified by the minimum value of free energy. In general we get the following three cases with S, σ and τ:

i) $\tau = \sigma = S = 0$, no order characteristic of the isotropic liquid phase;

ii) $\tau = 0$, $\sigma = 0$, $S \neq 0$, orientational order only, the theory reduces to the MS theory for the nematic phase; and

iii) $\tau \neq 0$, $\sigma \neq 0$, $S \neq 0$, orientational and translational order characteristic of the smectic A phase.

One can also predict the nature of the smectic to nematic phase transition observing McMillan ratio (T_{NA}/T_{NI}). If (T_{NA}/T_{NI})>0.87 then the SmA – N transition is of first order and if (T_{NA}/T_{NI})< 0.87 then it is of the second order. Here T_{NA} and T_{NI} are the SmA – N and N – I transition temperatures respectively.

X-Ray diffraction from liquid crystalline phases

One of the powerful and widely used techniques used for the characterization of various mesophases is the x-ray diffraction technique. Structural investigations of the mesophases and study of various microscopic physical quantities and their variation with temperature is possible by this method.X-ray diffraction studies from liquid crystalline mesophases have been done by several authors [32-40].

Let us consider a basic scattering experiment as shown in **Figure 2.2.** The incident as well as the scattered wave vectors have a magnitude $|\mathbf{K}_s| = |\mathbf{K}_i| = 2\pi / \lambda$, where λ is the wavelength of the incident radiation.

The scattering wave vector is given by

$$\mathbf{Q} = \mathbf{K}_s - \mathbf{K}_i \,, \qquad Q = |\mathbf{Q}| = \frac{4\pi}{\lambda}\sin\theta \tag{2.9}$$

where 2θ is the angle between $\mathbf{K}_s$ and $\mathbf{K}_i$.

The scattering of the incident radiation by a centre at **r** is described, relative to the initial amplitude, by the scattering amplitude

$$f \exp(i\mathbf{Q}.\mathbf{r}),$$

where f is the scattering power. For N such scattering centers the scattering amplitude is

$$F(\mathbf{Q}) = \sum_{j=1}^{N} f_j \exp(i\mathbf{Q}.\mathbf{r}_j) \tag{2.10}$$

where $\mathbf{r}_j$ is the position of the j^{th} scattering centre.

The scattering amplitude for a continuous distribution of the scattering centers is

$$F(\mathbf{Q}) = \int \rho(\mathbf{r}) \exp(i\mathbf{Q}.\mathbf{r}) d\mathbf{r} \tag{2.11}$$

where $\rho(r)$ is the time averaged electron density.

For a single isolated atom (2.11) can be written as

$$f(\mathbf{Q}) = \int \rho_a(\mathbf{r}) \exp(i\mathbf{Q}.\mathbf{r}) d\mathbf{r}$$

and it is called the atomic scattering amplitude. For a group of atoms, for which

$$\rho(\mathbf{r}) = \sum_{j=1}^{N} \rho_j(\mathbf{r} - \mathbf{r}_j)$$

this leads to

$$F(\mathbf{Q}) = \sum_{j=1}^{N} f_j(\mathbf{Q}) \exp(i\mathbf{Q}.\mathbf{r}_j) \qquad (2.12)$$

This is almost identical to (2.10). The diffraction by a group of atoms may be taken as diffraction by a set of points, if the variation in the atomic scattering amplitude is taken in account.

The scattered intensity at a particular point in **Q**-space is given by

$$I(\mathbf{Q}) = |F(\mathbf{Q})|^2$$

For molecular liquids it is convenient to separate the amplitude due to the molecular structure from the total scattering amplitude [41]. Accordingly (2.12) can be written as

$$F(\mathbf{Q}) = \sum_{k,m} f_{km}(\mathbf{Q}) \exp[i\mathbf{Q}.(\mathbf{r}_k - \mathbf{R}_{km})] \qquad (2.13)$$

where $\mathbf{r}_k$ gives the position of the centre of mass of the molecule 'k', and $\mathbf{R}_{km}$ is the position of the atom 'm' within that molecule, f_{km} is the atomic scattering factor of the atom 'm' in the molecule 'k'. Using (2.13) the general scattering intensity from a set of molecules is

$$I(\mathbf{Q}) = \sum_{k,l,n,m} \langle f_{k,m}(\mathbf{Q}) f_{ln}^*(\mathbf{Q}) \exp[i\mathbf{Q}.(\mathbf{r}_k - \mathbf{r}_j)] \exp[i\mathbf{Q}.(\mathbf{R}_{ln} - \mathbf{R}_{km})] \rangle \qquad (2.14)$$

where the brackets indicate statistical average over the constituent molecules of the liquid. The intensity given in (2.14) can be written as

$$I(\mathbf{Q}) = I_m(\mathbf{Q}) + D(\mathbf{Q})$$

where the molecular structure factor $I_m(\mathbf{Q})$ and the interference factor $D(\mathbf{Q})$ are given by

$$I_m(\mathbf{Q}) = \sum_k \langle \sum_{m,n} f_{km}(\mathbf{Q}) f_{kn}^{*}(\mathbf{Q}) \exp[i\mathbf{Q}.(\mathbf{R}_{kn} - \mathbf{R}_{km})] \rangle$$

$$= N\langle \left| \sum_m f_{km} \exp(-i\mathbf{Q}.\mathbf{R}_{km}) \right|^2 \rangle \qquad (2.15)$$

$$D(\mathbf{Q}) = \langle \sum_{k \neq l} \exp(i\mathbf{Q}.\mathbf{r}_{kl}) \sum_{m,n}' \langle f_{km}(\mathbf{Q}) f_{ln}^{*}(\mathbf{Q}) \exp[\mathbf{Q}.(\mathbf{R}_{ln} - \mathbf{R}_{km})] \rangle \rangle \qquad (2.16)$$

where $\mathbf{r}_{kl} = \mathbf{r}_k - \mathbf{r}_l$

The term $I_m(\mathbf{Q})$ gives the scattered intensity which would be observed from a dilute gas of identical molecules. $D(\mathbf{Q})$ contains information about correlation in both positional and orientation of different molecules. For example, it contains information regarding (i) apparent molecular lengths in nematics, (ii) layer thickness in smectics, (iii) average lateral distance between the molecules, (iv) correlation lengths, (v) tilt angle, (vi) molecular packing, (vii) orientational distribution function, (viii) order parameters $\langle P_2 \rangle$, $\langle P_4 \rangle$ ... etc., (ix) bond orientational order parameter, (x) layer order parameters τ and $\langle z^2 \rangle$ in Sm-A and (xi) critical exponents.

Methods of determination of some of these parameters relevant to the present study have been described later.

Experimental technique and data analysis

Identification of the Mesophases

All liquid crystalline phases are of importance from either theoretical point of view or from the view point of technological applications. Hence it is very important to identify the types of mesophases that are exhibited by a compound or a mixture.

The identification of liquid crystal phase type is usually done by several techniques viz., 1) Optical polarizing microscope 2) Differential scanning calorimetry 3) X-ray diffraction etc. The most widely used technique is the optical

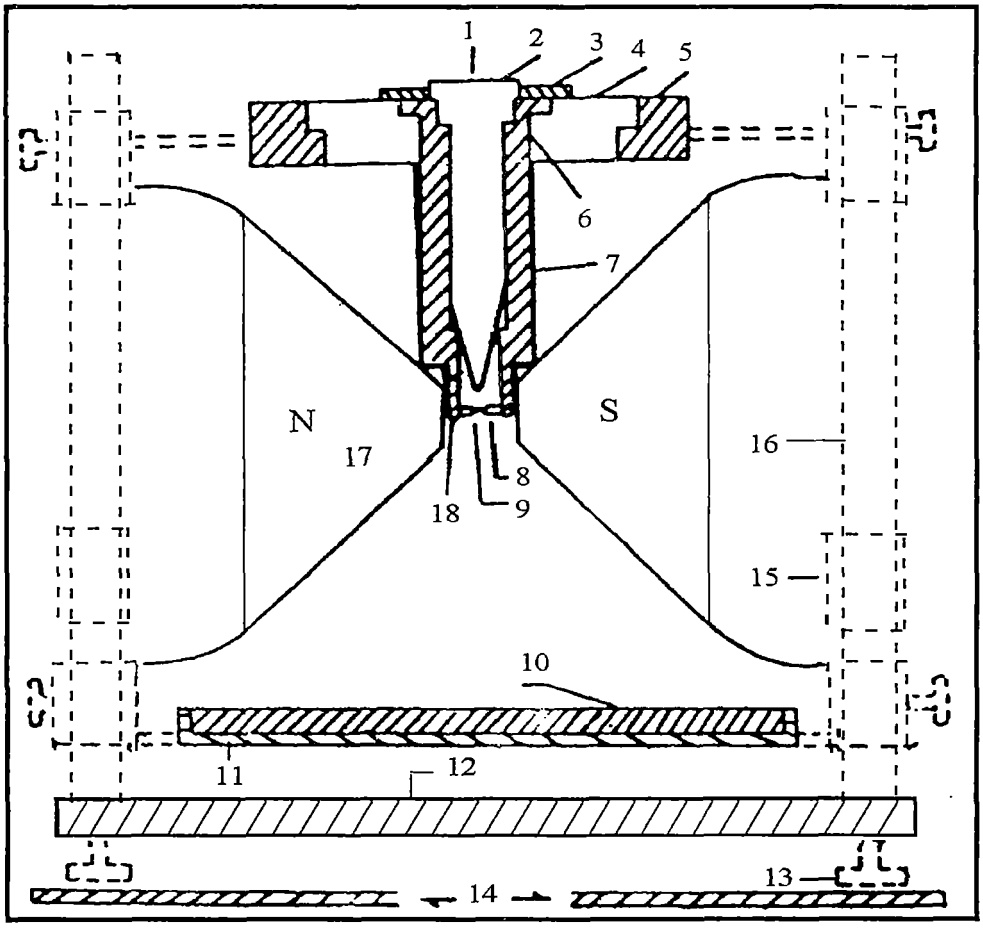

Figure 2.3 Schematic diagram of the X-ray Diffraction set up.
1.Entrance of x-ray 2. Collimator 3. Brass ring 4. Ring of syndanyo board 5. Brass ring 6. Cylindrical brass chamber 7. Asbestos insulation and heater winding 8. Specimen holder and thermocouple 9. Sample 10. Film cassette 11. Film cassette holder 12. Base plate 13. Levelling screw 14. Brass plates over the coils of the electromagnet 15.Removable spacer 16. Supporting brass stand 17. Pole pieces 18. Asbestos insulation.

polarizing microscope. Different mesophases exhibit distinct textures under a polarizing microscope, by observing these textures one can identify the phase transition temperatures as well as the nature of the phase. However, the identification of the mesophases by this technique is often difficult because similar textures might be exhibited by different phases or sometimes very subtle change in textures occur at transitions and hence requires the support of other techniques to finalize the phase type present.

Differential scanning calorimetry (DSC) is a useful technique and is usually always employed along with the optical microscopy. It reveals the transition temperatures by measuring the enthalpy change associated with a transition. However DSC cannot identify the type of liquid crystal phase, though the level of enthalpy change give some information about the degree of molecular ordering within a mesophase. Crystalline solid to liquid crystalline phase transition involves high enthalpy change (~30-40 $kJmol^{-1}$). But transition between two mesophases and mesophase to isotropic liquid transition are accompanied by much smaller enthalpy changes (~1-2 $kJmol^{-1}$).

The most reliable technique for the identification and classification of mesophases is X-ray diffraction analysis. However, good quality photograph from aligned samples are needed for this purpose. Alignment of the sample, which is usually done by the application of magnetic field, is difficult specially for higher order smectic phases.

Other techniques used to find the nature of a mesophase include neutron scattering [42], nuclear magnetic resonance [30,31,42-44], IR, Raman, UV-Visible spectroscopic studies [45], Fabry-Perot Etalon method[46] etc.

X-ray diffraction studies

The experimental set up used for the x-ray diffraction study is shown in **Figure 2.3**. The x-ray diffraction photographs are taken using nickel filtered CuK_{α} radiation, in a flat plate camera designed in our laboratory [47,48]. The sample is taken in a thin walled (~ 0.5mm) Lindemann glass capillary tube of 1mm diameter. The sample is aligned by cooling it slowly from the isotropic state to the desired

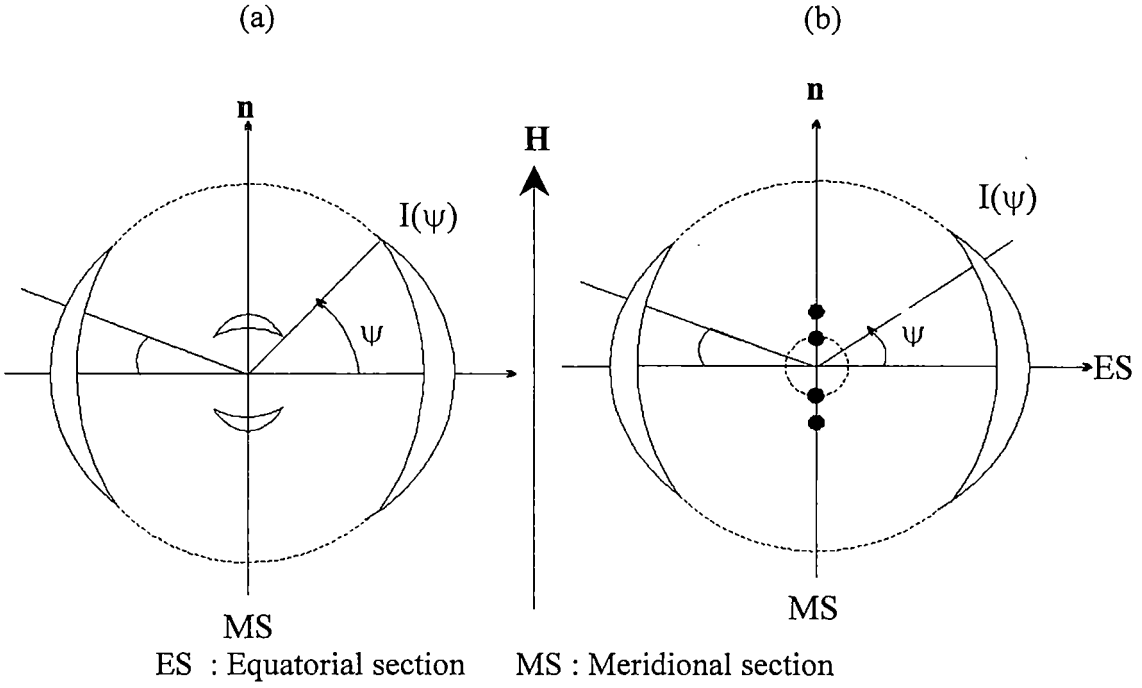

Figure 2.4. Schematic representation of the X-ray diffraction pattern of an oriented (a) nematic and (b) smectic A phase.

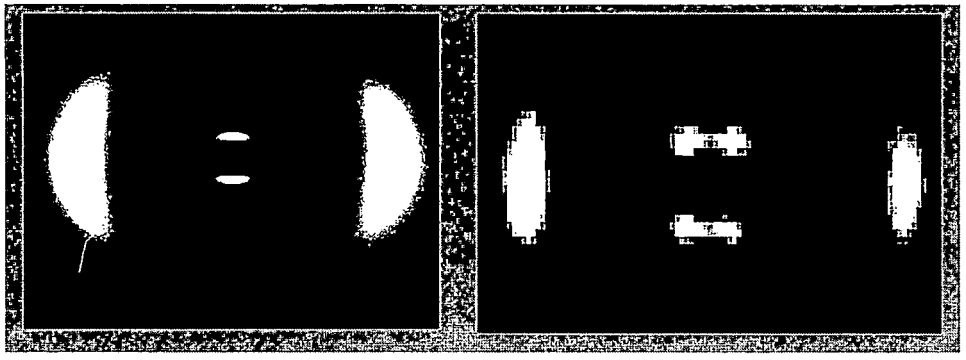

Ordinary nematic phase **Cybotactic nematic phase**

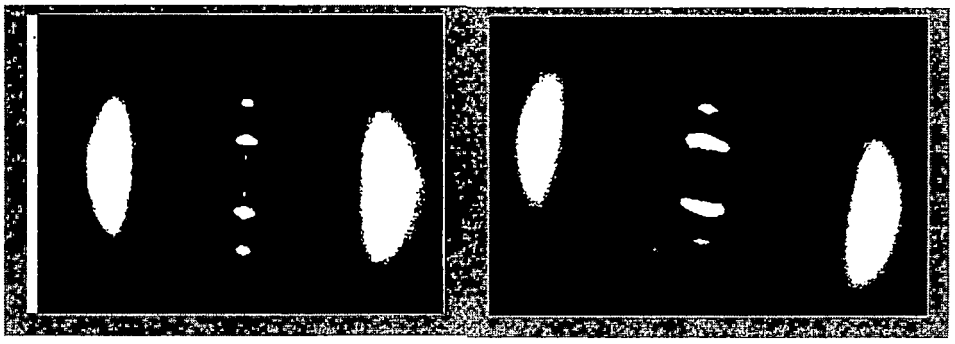

Smectic A phase **Smectic C phase**

Figure 2.5. Typical diffraction photographs of oriented nematic and smectic phases.

temperature in presence of a magnetic field of about 4-5 kGauss. X-ray photographs were taken at different temperatures by using a temperature controller, Indotherm 401- (India) within an accuracy of $\pm 0.5^0$C.

For the determination of the exact distance between the sample and the film, x-ray diffraction photograph of aluminium powder was taken. The Bragg's angle θ' corresponding to the (hkl) reflecting plane, can be determined by [49]

$$\sin\theta' = \frac{\lambda}{2a}\sqrt{h^2 + k^2 + l^2} \qquad (2.17)$$

where a is its lattice constant. Measuring the diameter of the diffraction rings corresponding to (111) and (222) reflections, the actual distance between the sample and the film can be found out from the relation

$$\tan 2\theta' = \frac{\text{radius of the ring}}{\text{sample to film distance}} \qquad (2.18)$$

Using the known sample to film distance, the Bragg angle (θ) for the peak corresponding to the parameter *l* and D of the liquid crystal sample are then calculated using the same relation (2.18).

The nature of the diffraction pattern depends upon the type of mesophase and hence from the x-ray diffraction photographs, different mesophases present in the sample can be characterized. The principal features of the x-ray diffraction pattern of nematic and smectic phases, which are oriented normal to the incident x-ray beam, are shown in **Figure 2.4** along with the actual diffraction photographs in **Figure 2.5**. The diffraction pattern consists of a combination of meridional and equatorial maxima normal to the director **n** (optic axis). The equatorial crescents form mainly due to the nearest neighbour intermolecular scattering and the corresponding Bragg's angle is a measure of the lateral intermolecular distance (D). The angular distribution of the x-ray intensity along the crescent give the orientational distribution function f(cosθ) and the order parameters $\langle P_L \rangle$ [50-53].

In the meridional direction, at a much smaller Bragg's angle, a pair of crescents is seen. These crescents are due to the correlations in the molecular arrangement along **n**. From the corresponding angle of diffraction the apparent molecular length (*l*) in N phase or the layer spacing (d) in smectic phase can be measured.

The average lateral distance between the neighbouring molecules (D) was calculated from the x-ray diffraction photographs by using the formula

$$2D \sin\theta = k\lambda$$

where 2θ is the Bragg angle for the equatorial diffraction, λ is the wavelength of the x-ray beam and 'k' is a constant which comes from the cylindrical symmetry of the system. For perfectly ordered state k=1.117 as given by de Vries [54,55]. As the variation of 'k' with $\langle P_2 \rangle$ is very small, the value of k = 1.117 is used for all our calculations.

The apparent molecular length or the layer thickness 'd' is calculated from the equation

$$2d \sin\theta = \lambda$$

where θ is the Bragg angle for the meridional diffraction crescents for an aligned sample and inner halo for unaligned sample.

The diffraction photographs were first digitized by using a scanner (hp scan jet 2200c). The digitized images were analyzed using the colour values of the pixels to obtain the apparent molecular length (*l*) or the smectic layer spacing (d) and the average intermolecular spacing (D). A GIS software **Idrisi 32** was used for analyzing the digital images.

Optical birefringence

Birefringence is the property exhibited by all anisotropic materials. When a light beam is incident on a uniaxial liquid crystalline compound two principal refractive indices (n_o and n_e) are observed. The first one, the ordinary refractive index n_o is observed, when the light beam is incident along the director **n**. If the light beam is perpendicular to the director and is polarized along **n** the

extraordinary refractive index n_e is observed. The optical anisotropy or birefringence is defined as $\Delta n = n_e - n_o$ which depends on the wavelength of the light used and the thermal state of the compounds [56]. Physical origin of the optical properties of liquid crystal has been detailed by Dunmur [57].

The optical anisotropy depends upon the molecular polarizability 'α' of the molecules and order parameter. For high order parameter, the molecules should be linear and have a long and rigid core. Molecules that consist of high polarizability units such as aromatic rings in the core, tolane linking groups and terminal cyano groups have a high birefringence. Conversely, a low birefringence is exhibited by molecules that are deficient in these types of groups and usually consist of alicyclic groups and terminal alkyl chains. The molecular polarizability 'α' can be determined by knowing the value of internal field, i.e., the average field acting on an individual molecule. But the Lorenz-Lorentz field, valid for isotropic phase, is not applicable for mesogens. Therefore, the Lorenz-Lorentz field, is replaced by the Vuks'[58] and Neugebauer's [59] internal fields.

Optical Polarisabilities from Refractive Index

Vuks' Method

Considering the internal field independent of molecular interaction, Vuks' derived the relations for polarizabilities associated with anisotropic molecules. In this case the effective molecular polarizabilities α_o and α_e, perpendicular and parallel to the direction of molecular axes, are related to n_o and n_e by the following equations:

$$\alpha_o = \frac{3}{4\pi N}\frac{n_o^2 - 1}{n^2 + 2} \qquad (2.19)$$

$$\alpha_e = \frac{3}{4\pi N}\frac{n_e^2 - 1}{n^2 + 2} \qquad (2.20)$$

where N is the number of molecules per unit volume and $n^2 = 1/3\ (n_e^2 + 2n_o^2)$. α_e and α_o can be calculated directly from the refractive index values.

Neugebauer's Method

By extending the Lorenz-Lorentz equations for an isotropic system to an anisotropic system, Neugebauer derived the following relations:

$$n_e^2 - 1 = 4\pi N\alpha_e\left(1 - N\alpha_e\gamma_e\right)^{-1} \tag{2.21}$$

$$n_o^2 - 1 = 4\pi N\alpha_o\left(1 - N\alpha_o\gamma_o\right)^{-1} \tag{2.22}$$

where N is the number of molecules per unit volume and γ_e and γ_o are the respective internal field constants for extraordinary and ordinary rays. The equations necessary for calculating polarisabilities α_o and α_e obtained from the above equations are:

$$\frac{1}{\alpha_e} + \frac{2}{\alpha_o} = \frac{4\pi N}{3}\left[\frac{n_e^2 + 2}{n_e^2 - 1} + \frac{2\left(n_o^2 + 2\right)}{n_o^2 - 1}\right] \tag{2.23}$$

$$\alpha_e + 2\alpha_o = \frac{9}{4\pi N}\left[\frac{n^2 - 1}{n^2 + 2}\right] \tag{2.24}$$

Solving the above two equations α_e and α_o values can be obtained.

Calculations of order parameters from polarizabilities

The principal polarizabilities, parallel and perpendicular to the direction of molecular axes, are related to the orientational order parameter $\langle P_2 \rangle$ [60,61]

$$\alpha_e = \bar{\alpha} + \frac{2}{3}\Delta\alpha S$$

$$\alpha_o = \bar{\alpha} - \frac{1}{3}\Delta\alpha S$$

Therefore $$\langle P_2 \rangle = \frac{\alpha_e - \alpha_o}{\alpha_{\parallel} - \alpha_{\perp}} \qquad (2.25)$$

where, $\bar{\alpha} = (2\alpha_o + \alpha_e)/3$, is the mean polarizability and $\Delta\alpha = \alpha_e - \alpha_o$ is the polarizability anisotropy. $\alpha_{\parallel}$ and $\alpha_{\perp}$ are the principal polarizabilities parallel and perpendicular to the long axes of the molecules in the perfectly ordered state i.e. $\langle P_2 \rangle = 1$ which are, however, not usually available.

To get the values of $(\alpha_{\parallel} - \alpha_{\perp})$ in the solid state is, the widely used Haller's extrapolation procedure is adopted [62]. A graph is plotted with log $(\alpha_e - \alpha_o)$ vs. log $(T_c - T)$ which should be a straight line. This line is extrapolated up to log (T_c), giving the value of $(\alpha_e - \alpha_o)_{T=0} = (\alpha_{\parallel} - \alpha_{\perp})$. Here T_c corresponds to the N-I transition temperature.

Measurement of refractive indices

The refractive indices n_o and n_e, corresponding to the ordinary and extraordinary rays, are measured by thin prism technique. Thin prisms are made by two optically plane glass plates. The glass plates were initially washed by nitric acid and clean water. After drying, the plates were again washed by acetone and then rubbed several times on white bond paper, parallel to one of the edges. The plates were then treated with a dilute solution of polyvinyl alcohol and then dried. The preferred direction on the substrates was obtained by rubbing the coated glass plates in the same direction on the bond paper. The prism was then formed, by keeping the treated surfaces inside and the rubbing directions parallel to the refracting edge of the prism. The side of the prism was then sealed on the three sides by using a high temperature adhesive. The angles of the prisms were kept less than 1° by using a thin glass spacer. The prisms were then left to dry and it was baked for several hours. The details of the preparation of the prism are already reported by Zeminder *et al.* [63]. The sample was introduced inside the prism by melting a few crystals, at the top open side. Repeated heating and cooling produced a homogeneous sample with the molecules perfectly aligned having the optic axis parallel to the refractive edges. The prism was then placed inside a thermostated brass oven with a circular

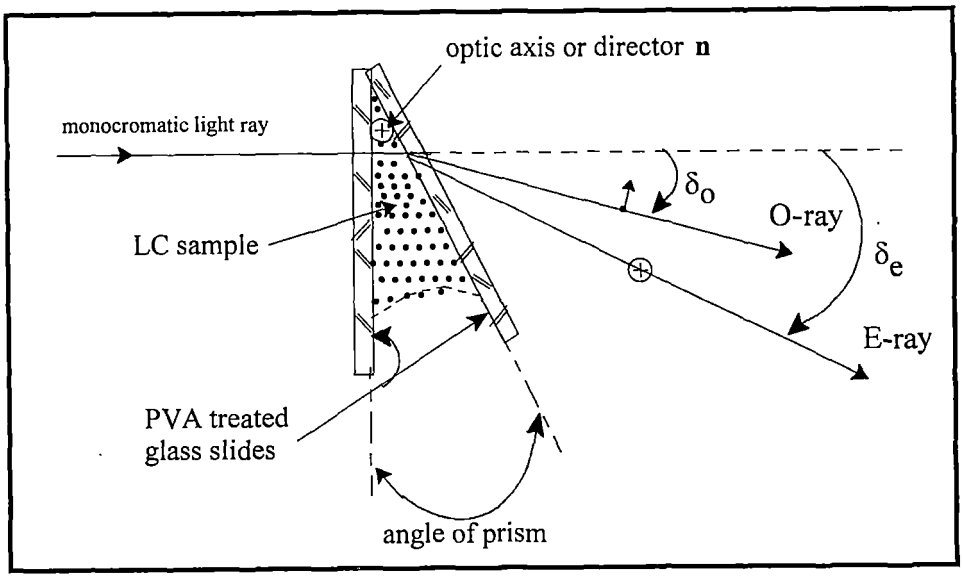

Figure 2.6. Schematic arrangement for the measurement of refractive indices.

aperture. The temperature of the oven was controlled by a temperature controller (Indotherm model 401) with an accuracy of ± 0.5°C. The refractive indices were measured by using a mercury lamp, a polarizer, a precision spectrometer, a wavelength selector, and a nicol prism. The refractive indices were measured for the wavelength λ_g=5461Å corresponding to the green light. A schematic diagram of the experimental set up for refractive indices measurements is shown in **Figure 2.6**.

Measurement of Density

The density of samples was measured by using a glass tube dilatometer of capillary type, a travelling microscope and temperature controller. A weighed sample of the liquid crystal was introduced inside the dilatometer in isotropic state. The bulb of the dilatometer was filled with mercury. The loaded dilatometer was placed in a thermostated glycerine bath. Sufficient time was allowed to reach the equilibrium at the desired temperature before taking each reading. The length of the liquid crystal column was measured at different temperatures during cooling from the isotropic state, with a travelling microscope. The densities were calculated after making the correction of glass expansion.

Study of Dielectric Permittivity

Dielectric studies of liquid crystals have proven to be very useful as a source of information about specific intermolecular interactions, molecular associations and molecular dynamics and relaxation mechanisms. The study of temperature dependence of the permittivity is also of considerable practical importance. The threshold voltage and other operational parameters of liquid crystal display devices depend on the anisotropy of the permittivity [64] and the multiplexity of matrix displays may be limited by the temperature dependence of the permittivity. Understanding the factors that determine the dielectric behaviour of liquid crystals will supplement the development of new materials with better display properties. So, the dielectric permittivities of liquid crystals have extensively been studied both experimentally and theoretically [65-70].

Maier and Meier(MM) theory of dielectrics for liquid crystals

Taking into account the polarization field in the medium W. Maier and G. Meier[71] extended the Onsager's theory [72] for isotropic dielectrics to nematics to correlate the dielectric properties with molecular parameters. According to Maier and Meier theory of nematics a molecule with polarizabilities $\alpha_{\parallel}$, $\alpha_{\perp}$ and permanent dipole moment μ and components $\mu_{\parallel} = \mu\cos\beta$, $\mu_{\perp} = \mu\sin\beta$, along and perpendicular to molecular long axis, is considered to be in a spherical cavity; β is the angle between the molecular long axis and the dipole moment μ. The environment of this molecule is taken as a continuum with the macroscopic properties of the dielectric. The dielectric permittivities $\varepsilon_{\parallel}$ and $\varepsilon_{\perp}$ along and perpendicular to the molecular long axis are then given by

$$\varepsilon_{\parallel} = 1 + 4\pi NhF\left\{\bar{\alpha} + \frac{2}{3}\Delta\alpha S + F\frac{\langle\mu_{\parallel}^2\rangle}{kT}\right\} \tag{2.26}$$

$$\varepsilon_{\perp} = 1 + 4\pi NhF\left\{\bar{\alpha} - \frac{1}{3}\Delta\alpha S + F\frac{\langle\mu_{\perp}^2\rangle}{kT}\right\} \tag{2.27}$$

with $$\langle\mu_{\parallel}^2\rangle = \frac{\mu^2}{3}\left[1 - (1 - 3\cos^2\beta)S\right]$$

$$\langle\mu_{\perp}^2\rangle = \frac{\mu^2}{3}\left[1 + \frac{1}{2}(1 - 3\cos^2\beta)S\right].$$

So that,

$$\Delta\varepsilon = \varepsilon_{\parallel} - \varepsilon_{\perp} = 4\pi NhF\left\{\Delta\alpha - F\frac{\mu^2}{2kT}(1 - 3\cos^2\beta)\right\}S, \tag{2.28}$$

$$\bar{\varepsilon} = \frac{\varepsilon_{\parallel} + 2\varepsilon_{\perp}}{3} = 1 + 4\pi NhF\left\{\bar{\alpha} + F\frac{\mu^2}{3kT}\right\} \tag{2.29}$$

Also, for isotropic state, when S=0, one gets the permittivity

$$\varepsilon_{iso} = 1 + 4\pi NhF\left\{\alpha_{iso} + F\frac{\mu^2}{3kT}\right\} \tag{2.30}$$

where N = the particle density = $\rho N_A/M$, ρ = mass density, N_A=Avogadro's number, M = Molecular weight, S= the order parameter and $\bar{\alpha}$= mean polarizability given by

$$\bar{\alpha} = \frac{\alpha_{\parallel} + 2\alpha_{\perp}}{3} \qquad (2.31)$$

$\Delta\alpha$ = polarizability anisotropy = $\alpha_{\parallel}$-$\alpha_{\perp}$, α_{iso} being the polarizability in the isotropic state; h and F are respectively the cavity field factor and the reaction field factor and are given by

$$h = \frac{3\bar{\varepsilon}}{2\bar{\varepsilon}+1} \qquad \text{and} \qquad F = \frac{1}{(1-\bar{\alpha}f)}$$

Here, f, called Onsager factor, is given by

$$f = \frac{8\pi}{3} N \frac{\bar{\varepsilon}-1}{2\bar{\varepsilon}+1}$$

The equations (2.26) for $\varepsilon_{\parallel}$ and $\varepsilon_{\perp}$ are often used to compute the effective dipole moment of the molecules and its orientation with the molecular long axis.

Maier-Maier's equations satisfactorily explain many essential features of the permittivity of liquid crystals consisting of polar molecules.

Dipole-Dipole Correlation Factor

Further insight into the phase structure may be obtained if the dipole-dipole correlation factor (g_λ), as defined below, is calculated.

$$g_\lambda = \frac{\langle \sum_{i \neq j} (\mu_\lambda)_i (\mu_\lambda)_j \rangle}{\langle \mu_\lambda^2 \rangle} \qquad (2.32)$$

This factor g_λ takes into account the correlation between the neighbouring dipole

moments only and the subscript λ refers to axes || and ⊥ to the nematic director. The ensemble averages of the || and ⊥ components of the molecular dipole moments are calculated following the procedure of Bata and Buka [73].

As noted earlier, short-range dipole-dipole interactions are not considered in Maier-Meier theory [71]. The Kirkwood-Fröhlich theory for isotropic liquid dielectrics [68,74] provides a formula in which these short-range effects are considered. Bordewijk and de Jeu [75-78] extended this idea to anisotropic media with uniaxial symmetry and used it to find dipole-dipole correlation factor for nematic liquid crystals. Their model was based on the observation that the square of birefringence (Δn^2) and the product of the density (ρ) and order parameter (S) is linearly proportional. Bata and Buka [73] later obtained the following relation between the low and high frequency dielectric constants:

$$\varepsilon_\lambda - \varepsilon_{\infty\lambda} = \frac{4\pi N \varepsilon_\lambda (\varepsilon_{\infty\lambda}+2)^2}{9kT\,(2\varepsilon_\lambda + \varepsilon_{\infty\lambda})} \langle \mu_\lambda^2 \rangle f_\lambda(\varepsilon, \Omega_\lambda^\varepsilon) g_\lambda \qquad (2.33)$$

where

$$f_\lambda(\varepsilon, \Omega_\lambda^\varepsilon) = \frac{2\varepsilon_\lambda + \varepsilon_{\infty\lambda}}{\varepsilon_\lambda - (\varepsilon_\lambda - \varepsilon_{\infty\lambda})\Omega_\lambda^\varepsilon} \qquad (2.34)$$

Here $\Omega^\varepsilon_\lambda$ is a factor which depends on the dielectric anisotropy of the system. For positive dielectric anisotropy [76] one has

$$\Omega_{||}^\varepsilon = \frac{\varepsilon_{||}}{\varepsilon_{||} - \varepsilon_\perp} - \frac{\varepsilon_{||} \cdot \varepsilon_\perp^{\frac{1}{2}}}{(\varepsilon_{||} - \varepsilon_\perp)^{3/2}} \tan^{-1}\left(\frac{\varepsilon_{||} - \varepsilon_\perp}{\varepsilon_\perp}\right)^{\frac{1}{2}} \qquad (2.35)$$

$$\Omega_\perp^\varepsilon = \frac{\varepsilon_{||} \varepsilon_\perp^{\frac{1}{2}}}{2(\varepsilon_{||} - \varepsilon_\perp)^{3/2}} \tan^{-1}\left(\frac{\varepsilon_{||} - \varepsilon_\perp}{\varepsilon_\perp}\right)^{\frac{1}{2}} - \frac{\varepsilon_\perp}{2(\varepsilon_{||} - \varepsilon_\perp)} \qquad (2.36)$$

For negative dielectric anisotropy

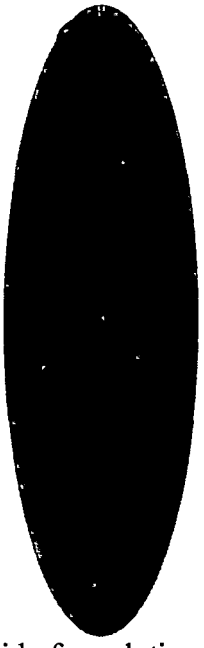

Figure 2.7 Model of ellipsoid of revolution having semi-major axis 'a' and semi minor axis 'b' of a liquid crystal molecule.

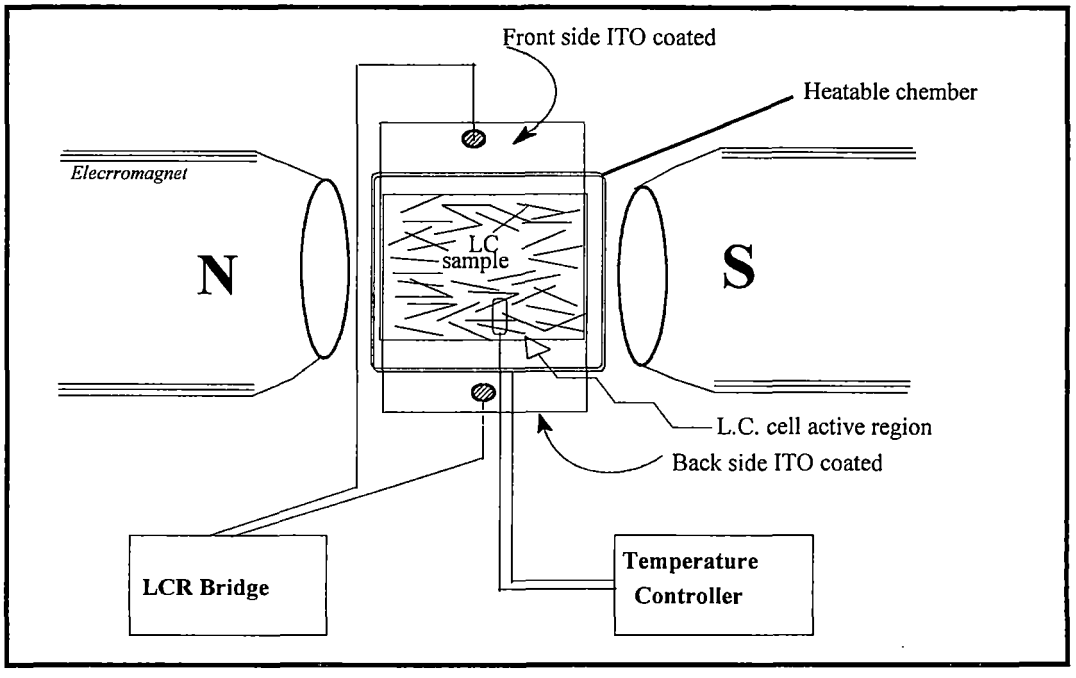

Figure 2.8. Schematic diagram of experimental set up for the dielectric constant measurement.

$$\Omega_{\parallel}^{\varepsilon} = \frac{\varepsilon_{\parallel}\varepsilon_{\perp}^{\frac{1}{2}}}{2(\varepsilon_{\perp}-\varepsilon_{\parallel})^{3/2}}\left(\ln\frac{\varepsilon_{\perp}^{\frac{1}{2}}+(\varepsilon_{\perp}-\varepsilon_{\parallel})^{\frac{1}{2}}}{\varepsilon_{\perp}^{\frac{1}{2}}-(\varepsilon_{\perp}-\varepsilon_{\parallel})^{\frac{1}{2}}}\right)-\frac{\varepsilon_{\parallel}}{\varepsilon_{\perp}-\varepsilon_{\parallel}} \tag{2.37}$$

$$\Omega_{\perp}^{\varepsilon} = \frac{\varepsilon_{\perp}}{2(\varepsilon_{\perp}-\varepsilon_{\parallel})}+\frac{\varepsilon_{\parallel}\varepsilon_{\perp}^{\frac{1}{2}}}{4(\varepsilon_{\perp}-\varepsilon_{\parallel})^{3/2}}\left(\ln\frac{\varepsilon_{\perp}^{\frac{1}{2}}-(\varepsilon_{\perp}-\varepsilon_{\parallel})^{\frac{1}{2}}}{\varepsilon_{\perp}^{\frac{1}{2}}+(\varepsilon_{\perp}-\varepsilon_{\parallel})^{\frac{1}{2}}}\right). \tag{2.38}$$

Hence, for both cases

$$\Omega_{\perp}^{\varepsilon} = \frac{1}{2}(1-\Omega_{\parallel}^{\varepsilon})$$

Average components of the effective dipole moment, $< \mu^2_{\parallel} >$ and $< \mu^2_{\perp} >$, appearing in equation (2.33) are evaluated from the following relations [73]:

$$\langle\mu_{\parallel}^2\rangle = \frac{1}{3}\left\{(2S+1)\left[\frac{\varepsilon_{\infty\parallel}+(1-\varepsilon_{\infty\parallel})\Omega_{\parallel}^{sh}}{\varepsilon_{\infty\parallel}}\right]^2\mu_{m\parallel}^2+(1-S)\left[\frac{\varepsilon_{\infty\perp}+(1-\varepsilon_{\infty\perp})\Omega_{\perp}^{sh}}{\varepsilon_{\infty\perp}}\right]^2\mu_{m\perp}^2\right\} \tag{2.39}$$

$$\langle\mu_{\perp}^2\rangle = \frac{2}{3}\left\{(1-S)\left[\frac{\varepsilon_{\infty\parallel}+(1-\varepsilon_{\infty\parallel})\Omega_{\parallel}^{sh}}{\varepsilon_{\infty\parallel}}\right]^2\mu_{m\parallel}^2+\frac{1}{2}(S+2)\left[\frac{\varepsilon_{\infty\perp}+(1-\varepsilon_{\infty\perp})\Omega_{\perp}^{sh}}{\varepsilon_{\infty\perp}}\right]^2\mu_{m\perp}^2\right\} \tag{2.40}$$

where the cavity field factor is calculated taking into account the shape factors (Ω_{λ}^{sh}) of ellipsoidal molecules with semi-major axis a and semi-minor axis b (**Figure 2.7**):

$$\Omega_{\parallel}^{sh} = 1-\omega^2+\frac{1}{2}\omega(\omega^2-1)\ln\frac{\omega+1}{\omega-1} \tag{2.41}$$

$$\Omega_{\perp}^{sh} = \frac{1}{2}\omega^2-\frac{1}{4}\omega(\omega^2-1)\ln\frac{\omega+1}{\omega-1} \tag{2.42}$$

so, $$\Omega_{\perp}^{sh} = \frac{1}{2}(1-\Omega_{\parallel}^{sh})$$

where $$\omega^2 = \frac{a^2}{a^2 - b^2} \tag{2.43}$$

The value of 2a is taken to be equal to apparent molecular length (l_{ap}) obtained from X-ray study and b is calculated by using the relation

$$b = \left[\frac{6M}{\pi N_A l_{ap} \rho}\right]^{\frac{1}{2}} \tag{2.44}$$

on the assumption that the volume occupied by a molecule in the LC phase is equal to the geometrical volume of the molecule[78]. They also used $\varepsilon_{\parallel\infty} = 1.05\ n_{\parallel}^2$ to take into account the atomic polarisation factor. Since, according to Kirkwood-Fröhlich theory, the effective value of molecular dipole moment is given by:

$$\mu^2_{eff.\parallel} = \frac{9kT}{4\pi N} \frac{(\varepsilon_{\parallel} - \varepsilon_{\infty\parallel})(2\varepsilon_{\parallel} + \varepsilon_{\infty\parallel})}{\varepsilon_{\parallel}(\varepsilon_{\infty\parallel} + 2)^2} \tag{2.45}$$

So, with the help of equation (2.33) we can rewrite equation (2.45) as

$$\mu^2_{eff\,\parallel} = f_{\parallel}(\varepsilon, \Omega_{\parallel}) g_{\parallel}(\varepsilon, T_{\parallel}) \langle \mu^2_{\parallel} \rangle$$

so that, $$g_{\parallel} = \frac{\mu^2_{eff\,\parallel}}{f_{\parallel} \langle \mu^2_{\parallel} \rangle} \tag{2.46}$$

Similarly for the perpendicular component we have:

$$\mu^2_{eff.\perp} = \frac{9kT}{4\pi N} \frac{(\varepsilon_{\perp} - \varepsilon_{\infty\perp})(2\varepsilon_{\perp} + \varepsilon_{\infty\perp})}{\varepsilon_{\perp}(\varepsilon_{\infty\perp} + 2)^2} \tag{2.47}$$

$$g_{\perp} = \frac{\mu^2_{eff\,\perp}}{f_{\perp} \frac{\langle \mu^2_{\perp} \rangle}{2}} \tag{2.48}$$

where the factor 2 arises due to rotational symmetry.

Equations (2.46) and (2.48) are used to calculate $g_{\parallel}$ and $g_{\perp}$ for uniaxial liquid crystals. Necessary computer programme has been written for this purpose.

Experimental Method for Measurement of Dielectric Permittivity Components

To measure the permittivities, a cell was constructed using two optically flat ITO coated conducting glass plates. The plates were separated by thin glass spacer. The cell was calibrated with CCl_4 and the dielectric constants ε for para-xylene was determined. The measured value agreed within 2% of standard values. Experimental sample was introduced into the cell as isotropic liquid. The cell was kept in a thermostated block, whose temperature was maintained by a temperature controller. Magnetic field of ~5KG was applied to align the sample. The cell is rotated by 90° with respect to the magnetic field such that a homeotropic alignment of the sample is achieved from a homogeneous one.

By applying electric field parallel and perpendicular to the director of the liquid crystal sample, capacitances C_e C_b and C_x was measured, for the cell filled with air, standard substance (para-xylene) and the liquid crystal sample respectively in parallel plate capacitor geometry, during cooling, by an LCR bridge (Systronics) at 1kHz. Components of the dielectric permittivities $\varepsilon_{\parallel}$ and $\varepsilon_{\perp}$, parallel and perpendicular to the director, were determined by using the relation

$$\varepsilon_x = 1 + \frac{(C_x - C_e)}{(C_b - C_e)}(\varepsilon_b - 1) \qquad (2.49)$$

where ε_b and ε_x are the relative permittivities of para-xylene and the liquid crystal substance; and that of air is taken as unity. The schematic diagram of the experimental set up designed and fabricated for dielectric measurements is shown in **Figure 2.8.**

Elastic Constants and Deformation Free Energy of Liquid Crystals

The macrosopic properties of liquid crystals such as electric permittivity, refractive indices, absorption coefficients, and orientational elastic constants can be described by continuum theory. Oseen [79] had described the distortional energy density in liquid crystals as a sum of specific curvature distortions of local optical

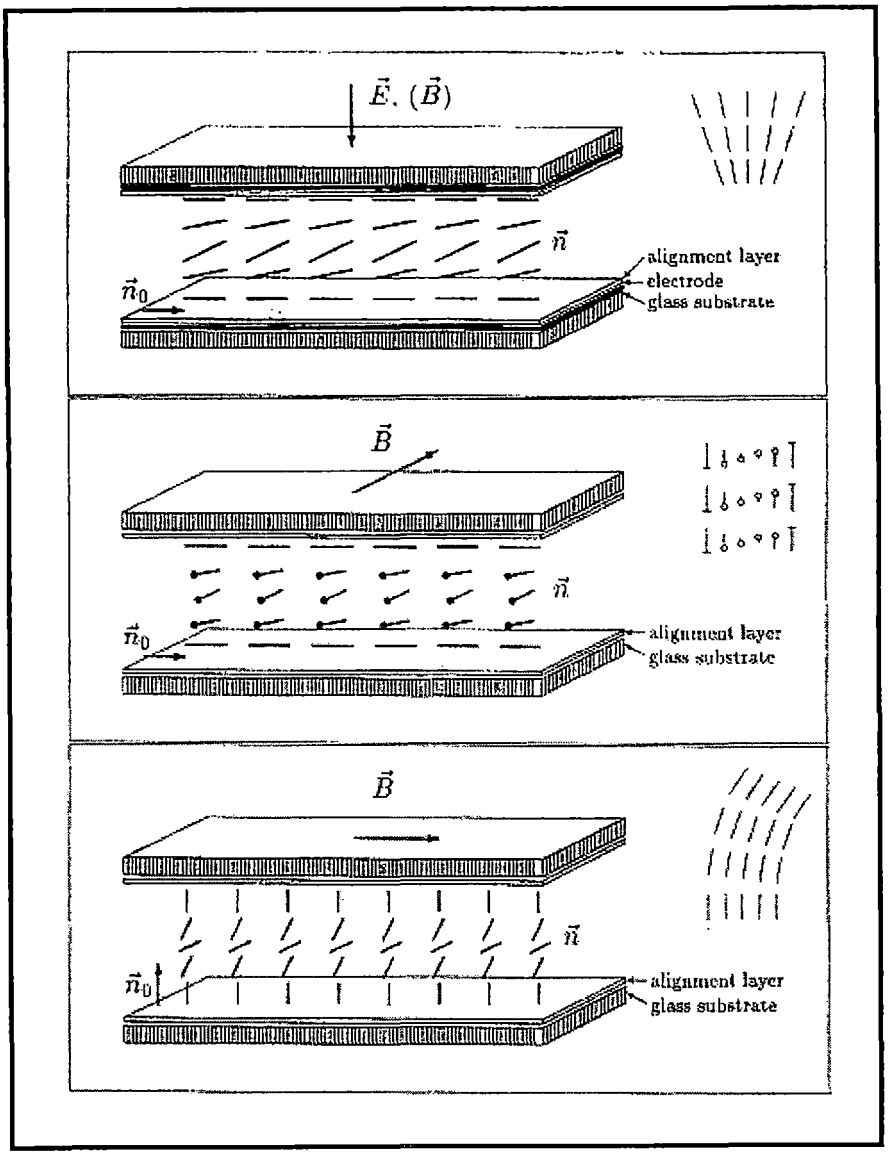

Figure 2.9. Cell geometries for the determination of splay (top), twist (middle) and bend (bottom) elastic constants from the Freedericksz threshold. Corresponding types of director deformations are sketched on the right.

[After Ref. 66, p63]

axis where every curvature is associated with its own elastic constants. Zocher [80] modified the Oseen view, that the distortions in a nematic liquid crystal takes place throughout the bulk and therefore is of continuous nature. Frank [81] reformulated parts of Oseen theory. Thus, the continuum theory developed by Zocher, Oseen and Frank can explain field induced effect of liquid crystals. A more general approach to the elastic properties has been given by Nehring and Saupe [82], Jahnig and Schmidt [83] as well as Martin, Parodi and Pershan[84]

If the liquid crystal is deformed so as to result in a splay by electrical or magnetic forces, a reactive elastic force will tend to restore the initial confirguration. The same phenomenon will occur for a twist deformation as well as for a bend deformation. The three types of director deformation are shown in **Figure 2.9**. The magnitude of their reactive forces is described by the elastic constants K_{11}, K_{22} and K_{33} respectively.

If F_d is the elastic free energy associated with the distortion of director $\mathbf{n}(\mathbf{r})$ from the state of uniform alignment $\mathbf{n}(\mathbf{r}) = \mathbf{n}_0$ then we may write [82]

$$F_d = \int d^3r \; f_d \qquad (2.50)$$

where the free energy density f_d is given by

$$f_d = \tfrac{1}{2}\{ K_{11} (\text{div } \mathbf{n})^2 + K_{22} (\mathbf{n} . \text{curl } \mathbf{n})^2 + K_{33} (\mathbf{n} \times \text{curl } \mathbf{n})^2 + K_{24} \text{ div}[(\mathbf{n}. \text{ grad}) \mathbf{n} - \mathbf{n} \text{ div } \mathbf{n}]\} \qquad (2.51)$$

where K_{11}, K_{22} and K_{33} are respectively the splay, twist and bend elastic constants. By the divergence theorem the term K_{24} contributes to only surface energy and therefore neglected in case of disclination free sample with strong anchoring boundary conditions [85].

If it is assumed that when a smectic A phase is distorted the number of layers within two points A and B remains constant, then

$$t_s^{-1}\int_A^B \mathbf{n}.d\mathbf{l} = \text{constant} \qquad (2.52)$$

where t_s^{-1} is the wavelength of the mass density wave given by

$$\rho(z)=\rho_o[1+\sqrt{1/2}\,|\,\psi_s\,|\cos(q_s z-\phi_s)] \qquad (2.53)$$

with complex order parameter

$$\psi_s = |\,\psi_s\,|\exp(i\phi_s) \qquad (2.54)$$

superposed parallel to **n** on the nematic order. The wavelength of the density wave $2\pi/q_s$ being of the order of one or two molecular lengths.[86].

For a closed curve C bounding a surface S

$$t_s^{-1}\int_C \mathbf{n}.d\mathbf{l} = t_s^{-1}\int_S (\text{curl}\,\mathbf{n}).d\mathbf{s} = 0 \qquad (2.55)$$

which implies that curl **n** must vanish and that K_{22} and K_{33} must diverge in the smectic A phase.

Hence $f_d = \frac{1}{2}\{ K_{11} (\text{div}\,\mathbf{n})^2 + \text{compressibility terms}$

For a layer with principal radii of curvature R_1 and R_2

$$\frac{1}{2} K_{11}(\text{div}\mathbf{n})^2 = \frac{1}{2} K_{11}(R_1^{-1} + R_2^{-1})^2 = 0 \qquad (2.56)$$

$$\text{if } R_1 = R_2 = \infty \text{ or } R_1 = R_2$$

which shows that K_{11} vanishes for flat layers and for saddle shaped layers with equal but opposite radii of curvature.

This shows that smectic A phases can distort from uniform alignment with flat layers and constant **n**. The development of such distortion on passing from aligned nematic into smectic phase may cause spurious change in the apparent values of macroscopic properties [85]. However, the K_{33}/K_{11} is also found to diverge near SmA-N transition due to formation of smectic clusters as pre-transitional effect [87].

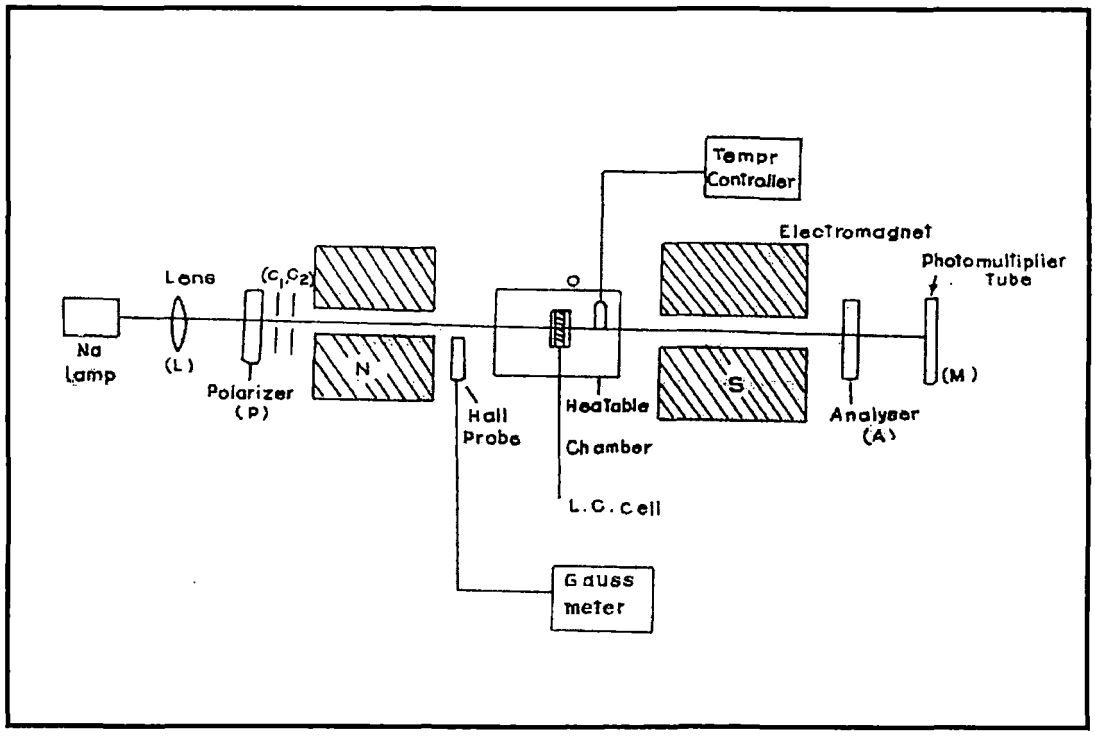

Figure 2.10. Experimental setup for the determination of elastic constants.

Freedericksz transition

A simple and convenient method of determining elastic constants is by Freedericksz transition. Several authors have reported the determination of elastic constants [88-93] by this technique. Here an external electric or magnetic field is applied to deform the thin layer of surface aligned nematic liquid crystal having a uniform director (**n**) pattern. The external field causes the molecules to align along the direction of the field, above a certain critical field for liquid crystals having positive anisotropy ($\Delta\chi$, $\Delta\varepsilon$ >0). Below the critical field the molecules remains surface aligned. This phenomenon is known as Freedericksz transition. From the geometry of arrangement, the splay, twist and bend elastic constants can be determined from Freedericksz transition in a magnetic field. The threshold magnetic field for all the three geometry can be obtained from

$$(H_c)_i = \pi/d\ (K_{ii}/\Delta\chi)^{1/2} \qquad (2.57)$$

Here i = 1,2,3 refers to splay, twist and bend deformations respectively, $\Delta\chi$ is the diamagnetic susceptibility anisotropy, $(H_c)_i$ is the respective threshold magnetic field and d is the thickness of the liquid crystal layer.

Experimental

The block diagram of the experimental set up for studying elastic constants is shown in **Figure 2.10**. Monochromatic beam of light from a sodium vapour lamp is passed through a lens L, polarizer P, and collimating circular slits C1 and C2 and allowed to incident on the liquid crystal sample. The sample is contained in a cell made of treated glass plates for surface alignment and mounted on a brass oven. The temperatures of the oven are measured and regulated with a thermocouple inserted in the oven and a temperature controller (Indotherm 401). The transmitted light intensity from the sample is detected by a photo multiplier tube (PMT) after passing through an analyzer. The current from the photomultiplier tube is measured with a nanoammeter. The polarizer and the analyzer are placed in crossed position. The

magnetic field H is applied perpendicular to the direction of the preferred orientation of the sample. The magnetic field is increased slowly so that the molecular orientations remain in equilibrium with the field. The intensity of the transmitted light is measured as a function of the applied magnetic field for any desired temperature. When the field H reaches a critical value H_c there is an abrupt change in the current, indicating the change in the optical properties of the sample. The critical field was measured with a sensitive Gaussmeter (Model DGM-102) within an accuracy of ±10 gauss.

The cells were made with two plane parallel glass plates and glass spacer. The glass plates were cleaned by cleaning agents and dried. For homogeneous alignment to measure the splay elastic constant (K_{11}) the inner surface of the glass plates were treated with 1% aqueous solution of polyvinyl alcohol and dried. The dried glass surface was rubbed unidirectionally with tissue paper. In case of homeotropic alignment to measure the bend elastic constants (K_{33}) the inner surfaces of the glass plates were treated with dilute solution of cetyltrimethyl ammonium bromide (CTAB) in acetone [94].

In case of twist deformation the threshold field cannot be detected along the twist axis. The state of polarization of the transmitted light is indistinguishable from that of the emerging beam from the untwist nematic. To measure K_{22} values of the twist deformation the total internal reflection method is employed.

Determination of Crystal Structures

For proper understanding and interpretation of several physical properties of liquid crystals a knowledge of the molecular structure in the crystalline state is very useful. The molecular conformation in the crystalline state predetermines the molecular organization in the mesomorphic state. Bernal and Crowfoot [95] in the early 1930's, made the first attempt to correlate the molecular arrangement in the mesomorphic state with the crystal structure of the mesogenic material. However, further studies had been very few for many years in the crystal structure determination. With the advent of computer programs in the late 70's, a large

number of structures of liquid crystal forming compounds have been determined most of which are nematogens. Crystal structures determined by the co-workers are given in references [96-104].

Preliminary survey on the present knowledge of the structure-property relationship is given by Bryan [105] and more recently by Haase and Athanassopoulou [106]. On the basis of the available results it can be stated that

(i) the molecules of the liquid crystalline compounds on heating adopt an arrangement some what similar to that in the crystals

(ii) the long and narrow molecules are more or less parallel and interleave one another to form an 'imbricated packing' in a nematogenic crystal

(iii) the molecules are found to be packed in parallel layers in a smectogenic crystal

Although the above picture is true in large number of known cases, the generalization must be made with caution since examples are also known where it is not true [106,107].

Theory of Crystal Structure Determination

The constituent atoms or molecules in a crystal are arranged in a regular and periodic manner with long range positional and orientational order. A unit cell can therefore be constructed, with edges given by three non coplanar vectors **a, b, c** and the angles α, β, γ between the edges. The diffraction by crystals results from a process in which x-ray are scattered by the electrons of the atoms without change in wavelength. The 2-D diffraction pattern therefore contains features where intensity varies as a function of position. From the positions of the diffraction features one can find the unit cell dimensions. To locate the positions of the individual atoms in the unit cell, the intensity of the diffracted pattern must be measured and analysed. If f_j be the amplitude scattered by the j-th atom at point $\mathbf{r}_j$ and if there are N such atoms within the cell, then the amplitude of the radiation scattered from the array of planes represented by the Miller indices (hkl) is given by [108],

$$F_{hkl} = \sum_{j=1}^{N} f_j \exp 2\pi i(hx_j + ky_j + lz_j) \qquad (2.58)$$

The quantity f_j is called scattering factor or form factor, F_{hkl} is known as the structure factor for the reflection hkl. $|F_{hkl}|$ is called the structure amplitude, is a pure number- number of electrons.

The above equation may also be written as

$$F_{\mathbf{H}} = \sum_{j=1}^{N} f_j \exp\left(2\pi i \mathbf{H}.\mathbf{r}_j\right)$$

As the atoms in the unit cell are at the positions of high electron density $\rho(\mathbf{r})$, so $F_{\mathbf{H}}$ can be expressed as

$$F_{\mathbf{H}} = \int_V \rho(\mathbf{r}) \exp(2\pi i \mathbf{H}.\mathbf{r}_j)$$

where V is the volume of the unit cell. By Fourier transformation we have

$$\left.\begin{aligned} \rho(r) &= \frac{1}{V}\int_S F_H \exp(-2\pi i H.r)\,ds \\ \rho(r) &= \frac{1}{V}\sum_h\sum_k\sum_l F_H \exp(-2\pi i H.r) \end{aligned}\right\} \qquad (2.59)$$

If we could obtain a large number of $F_{\mathbf{H}}$ by the diffraction experiment, we could have directly derived the crystal structure by Fourier summation. However, from diffraction experiments we get a set of diffracted intensities ($I_{\mathbf{H}}$) from different hkl planes. From these values we can get the magnitude of the structure factors $|F_{\mathbf{H}}|$, but not their phases $\phi_{\mathbf{H}}$ and this constitutes the phase problem in crystallography. To overcome this problem, there are four main methods viz., (1) *Patterson function*, (2) ***Direct methods***, (3) *Isomorphous replacement technique* and (4) *Anomalous scattering method.* Here we discuss the direct method [109], since the structure of a liquid crystalline compound is determined by this method.

Direct methods

Direct methods of crystal structure determine phases $\phi_{\mathbf{H}}$ directly from the observed intensities (I_{obs}) by probabilistic calculations. Following the work of

Herbert Hauptman and Jerome Karle the direct methods are very efficient in solving crystal structures especially of low molecular weight organic compounds.

Different computer programs are now available for solving crystal structures by direct methods viz., MULTAN [110], SIMPEL [111], SHELX[112], XTAL[113], SIR 92 [114], NRCVAX [115], SAPI [116], MITHRIL[117] etc. Some of these have been described in several books and monographs [118-122].

A systematic account of the development of the direct methods is beyond the scope of this thesis. Only the basic principles and working formulae will be discussed here.

Structure Invariant and Seminvariants

A structure invariant is defined as a quantity that is independent of the shift of the origin of the unit cell.

The intensities $I_{\mathbf{H}}$ of reflections i.e. $|F_{\mathbf{H}}|^2$ are structure invariants. However the structure factor itself is not structure invariant, otherwise the phase problem would not have exist. This is because, for any shift in the origin by, say, $\Delta\mathbf{r}$ the phase of $F_{\mathbf{H}}$ changes by $-2\pi\mathbf{H}.\Delta\mathbf{r}$ radians while the amplitude remains invariant. Similarly it can be shown that that $|F_{\mathbf{H}}|^2$ is structure invariant. Though individual phases depend on the structure and choice of origin, some combinations of them is structure invariant. For example, if $\mathbf{H}_1+\mathbf{H}_2+\mathbf{H}_3=0$ then $\phi_{\mathbf{H}1}+\phi_{\mathbf{H}2}+\phi_{\mathbf{H}3}$ is structure invariant for every space group. It follows directly from the fact that the product $F_{-\mathbf{H}}F_{\mathbf{K}}F_{\mathbf{H}-\mathbf{K}}$ is an invariant. Since the moduli of the structure factors are invariant themselves, the angular part of $F_{-\mathbf{H}}F_{\mathbf{K}}F_{\mathbf{H}-\mathbf{K}}$ is also invariant i.e. $\phi_{-\mathbf{H}} + \phi_{\mathbf{K}} + \phi_{\mathbf{H}-\mathbf{K}} = \phi(\mathbf{H},\mathbf{K}) = \phi_3$ is invariant.

The structure seminvariants are quantities that do not change value on transfer from one special origin to another. The structure seminvariants are those linear combinations of the phases whose values are uniquely determined by the crystal structure alone, when the choice of origin is restricted within permissible values. It originates from space group symmetry. For example in space group $P\bar{1}$, the linear combination $2\phi_{-\mathbf{H}} + \phi_{2\mathbf{H}}$ is a structure invariant for any reciprocal vector

H. For each space group they have to be derived separately. In any space group any structure invariant is also a structure seminvariant, but reverse is always not true. A complete theory is given in a series of papers by Hauptman and Karle[123-125] and by Schenk [126].

Structure Determination Procedures

The intensity data are collected from the single crystal X-ray diffractometer using usually CuK_α/MoK_α radiation. The intensity data are corrected for Lorentz polarization factors [127]. The intensities are converted into the structure factors on an absolute scale by determining the scale factor by the method introduced by A. J. C Wilson [128]. To take into account the thermal vibrations of the atoms the temperature factors are also obtained during the process. Then the following steps are taken:

1. Estimation of normalised structure factors |E|'s from $|F_{obs}|$ values
2. Set up of phase relationships via structure invariants and seminvariants, starting phase determination, phase extension and refinement
3. Calculation of figure of merit of different phase sets
4. Production of E-map by Fourier method and their interpretation
5. Refinement of structures through Fourier synthesis, Difference Fourier synthesis and Least-square refinement techniques.

Estimation of |E|'s from $|F_{obs}|$ values

In direct methods the phases of the structure factors are estimated directly from the structure amplitudes so the decrease of the atomic scattering factor with increasing scattering angle has to be removed. The observed $|F_H|$ is therefore modified so that they correspond to the hypothetical diffracted waves which would be obtained if atoms were stationary point atoms at rest. The modified structure factor, called 'Normalised structure factor' (E_H) , is defined as,

$$|E_{\mathbf{H}}|^2 = \frac{|F_{\mathbf{H}}|^2}{\varepsilon \sum_{j=1}^{N} f_j^2} = \frac{I_h}{\langle I \rangle}$$

and $$\left\langle |E_{\mathbf{H}}|^2 \right\rangle = 1$$

where ε is an integer characteristic of the space group symmetry.

Set up of phase relationships, starting phase determination, phase extension and refinement

At the initial stage, phases of only the strongest reflections are determined. In practice a suitable number of reflections (4 x no. of independent atoms + 100) are chosen. If the crystal is triclinic or centrosymmetric, more reflections may be required.

The most commonly used phase relation is a three phase structure invariants based on the positivity of electron density criterion, as proposed by Karle and Karle[125]:

$$\phi_{\mathbf{H}} \approx \phi_{\mathbf{K}} + \phi_{\mathbf{H}-\mathbf{K}} \qquad (2.60)$$

which for centrosymmetric structure is expressed by signs as

$$S(\mathbf{H}) \approx S(\mathbf{K})\, S(\mathbf{H}-\mathbf{K}) \qquad (2.61)$$

Relation (2.60) is used to generate phases $\phi_{\mathbf{H}}$ when the values of the phases on the right-hand side are known and it is used in a cyclic manner to propagate the phases to all the selected reflections. These relations are probability relations and the probability is high when the reflections have large |E| values in addition to satisfying the criterion $\mathbf{H} + \mathbf{K} + \mathbf{L} = 0$. These are called Σ_2 phase relations. Probability of the phase of **H** being equal to the sum of the phases of **–H** and **H-K** is given by the following relations. In centrosymmetric case [129]:

$$P_+(\mathbf{H},\mathbf{K}) = \frac{1}{2} + \frac{1}{2}\tanh\left[\frac{1}{2}k(\mathbf{H},\mathbf{K})\right] \qquad (2.62)$$

In non-centrosymmetric case [130]:

$$P[\phi(\mathbf{H},\mathbf{K})] = \frac{\exp\{k(\mathbf{H},\mathbf{K})\cos[\phi(\mathbf{H},\mathbf{K})]\}}{2\pi I_o\{k(\mathbf{H},\mathbf{K})\}} \tag{2.63}$$

where I_0 is a zero-order modified Bessel function of the first kind.

Now the question arises about deciding the phase of a particular reflection when there are several pairs of known phases, the estimate from each of which might be well different. The answer to this important problem was given by Karle and Hauptman[131] in 1956. They introduced the tangent formula

$$\tan\phi_{\mathbf{H}} \approx \frac{\sum_{\mathbf{K}} k(\mathbf{H},\mathbf{K})\sin(\phi_{\mathbf{K}} + \phi_{\mathbf{H}-\mathbf{K}})}{\sum_{\mathbf{K}} k(\mathbf{H},\mathbf{K})\cos(\phi_{\mathbf{K}} + \phi_{\mathbf{H}-\mathbf{K}})} = \frac{B(\mathbf{H})}{A(\mathbf{H})} \tag{2.64}$$

where $k(\mathbf{H},\mathbf{K}) = 2\sigma_3\sigma_2^{-\frac{3}{2}}|E_{\mathbf{H}}||E_{\mathbf{K}}||E_{\mathbf{H}-\mathbf{K}}|$

$$\sigma_n = \sum_{j=1}^{N} Z_j^n$$

Z_j being the atomic number of the j^{th} atom in a unit cell containing a total of N atoms. For identical atoms $\sigma_3\sigma_2^{-\frac{3}{2}} = N^{-\frac{1}{2}}$.

In order to use the tangent formula to obtain a new phase, the value of some phases have to be known and put into the right -hand side of the tangent formula. The set of the known phases is called a starting set from which the tangent formula derives more and more new phases and refines them in a self-consistent manner. But in this way all phases cannot be determined with acceptable reliability. It is therefore useful at this stage to eliminate about 10% of these reflections whose phases are most poorly defined by the tangent formula (2.64). An estimate of the reliability of each phase is obtained from $\alpha(\mathbf{H})$:

$$\alpha(\mathbf{H}) = \{A(\mathbf{H})^2 + B(\mathbf{H})^2\}^{\frac{1}{2}} \tag{2.65}$$

when the relation (2.65) contains only one term, as it may in the initial stages of the phase determination, then $\alpha(\mathbf{H}) = k(\mathbf{H},\mathbf{K})$.

The larger the value of $\alpha(\mathbf{H})$, the more the reliable is the phase estimate. The relation between $\alpha(\mathbf{H})$ and the variance is given by Karle and Karle [125], in 1966, as

$$\sigma^2(\mathbf{H}) = \frac{\pi^2}{3} + 4\sum_{t=1}^{\infty} \frac{(-1)^t}{t^2} \frac{I_t\{\alpha(\mathbf{H})\}}{I_0\{\alpha(\mathbf{H})\}}$$

From (2.65) it can be seen that $\alpha(\mathbf{H})$ can only be calculated when the phases are known. However, an estimate of $\alpha(\mathbf{H})$ can be obtained from the known distribution of three phase structure invariants [130]. The estimated $\alpha(\mathbf{H})$ at the initial stage is given approximately by

$$\alpha_{est}(\mathbf{H}) = \sum_{\mathbf{K}} k(\mathbf{H},\mathbf{K}) \frac{I_1\{k(\mathbf{H},\mathbf{K})\}}{I_0\{k(\mathbf{H},\mathbf{K})\}} \qquad (2.66)$$

As the tangent phasing process is usually initiated with a few 'known' phases so to fix the origin and enantiomorphs is the first step in phase extension. This is done imposing the condition in terms of structure factor seminvariant phases. The selection of starting phases is critical to the success of the multisolution methods. The generator reflections are sorted by a convergence-type process by Germain, Main and Woolfson[110] which maximises the connection between starting phases. At the end of the convergence procedure a number of reflections, sufficient to fix the origin and the enantiomorphs whose phases are known, are obtained. A few other reflections are also chosen to which different phase values are assigned (either numerically or symbolically) to create different starting points for phase extension through Σ_2 relations. The strength of convergence procedure is that it ensures, as far as possible, that the initial phases will develop through strong and reliable phase relationships. For each starting phase set, phases of all the selected strong reflections are generated and refined as explained in earlier section. Thus we get a multiple phase sets.

Calculation of figure of merit of the generated phase sets

When a number of sets of phases have been developed, it is necessary to rank them according to some Figure-of-Merit (FOM), prior to computing a

Fourier map (in this case E-map). Combining all weights from various FOM viz., Absolute Figure-of-Merit (ABSFOM), Relative Figure-of-Merit (RFOM), R-factor Figure-of-Merit (RFAC), Psi (zero) Figure-of-Merit (PSIO) etc. Combined Figure-of-Merit (CFOM) are calculated for each set. The most likely correct sets of phases are those with the highest value of CFOMs.

E-map calculation and interpretation

Using the best phase set, E-maps are calculated using equation 2.53 at a large number of grid points covering the entire unit cell. The complete interpretation of the maps is done in three stages: peak search, separation of peaks into potentially bonded clusters and application of simple stereochemical criteria to identify possible molecular fragments.

The molecular fragments thus obtained can be compared with the expected molecular structure. The computer can thus present the user with a list of peaks and their interpretation in terms of the expected molecular structure quite automatically. It is also common practice to have an output of the picture of the molecule as an easy check on the structure the computer has found.

Refinement of structures through Fourier synthesis, Difference Fourier synthesis and Least-square refinement technique

Generally for refinement of a model structure (partial or complete) obtained from E-map we use following three methods, e.g., 1) Fourier synthesis, 2) Difference Fourier synthesis and 3) Least squares refinement [132,133] .

The Fourier synthesis gives the refined co-ordinates of the atoms and also tends to reveal the position of any atom that is not included in computing the structure factors using equation (2.58). The Difference Fourier map is very useful for correcting the position of an atom used in structure factor calculation. This is also very useful in locating H-atoms towards the final stages of refinement procedure.

An analytical method of refinement of great power and generality is that based on the principle of least squares. In brief, least-squares refinement

consists in using the squares of the differences between observed and calculated structure factors as a measure of their disagreement and adjusting the parameters so that the total disagreement is a minimum.

An agreement between the calculated structures factors F_c and those observed, F_o, indicates the degree of refinement. The most common method of assessing the agreement is calculating the residual or reliability index of the form

$$R = \frac{\sum\left(|F_o| - |F_c|\right)}{\sum|F_o|} \tag{2.66}$$

the summation being over all the reflections. Evidently, the lower the value of R, the better is the agreement. Another form of the residual of common use is

$$R_w = \left[\frac{\sum w\left(|F_o - F_c|^2\right)}{\sum w|F_o|^2}\right]^{\frac{1}{2}} \tag{2.67}$$

where the frequently used weight is,

$$w = \frac{1}{\sigma^2(F_o)}$$

$\sigma(F_o)$ being the standard deviation of F_o.

Measurements on Ferroelectric Liquid Crystals

Ferroelectric liquid crystals (FLCs) are the recent members of ferroelectric materials with fluid properties. Like their solid counterpart they have a Curie point, at which the bulk polarization vanishes. A Curie-Wiess law is often obeyed by the electric permittivity. However they are different from the solid ferroelectrics, in many other respects. Ferroelectricity in FLCs usually originates due the molecular-chiral asymmetry.

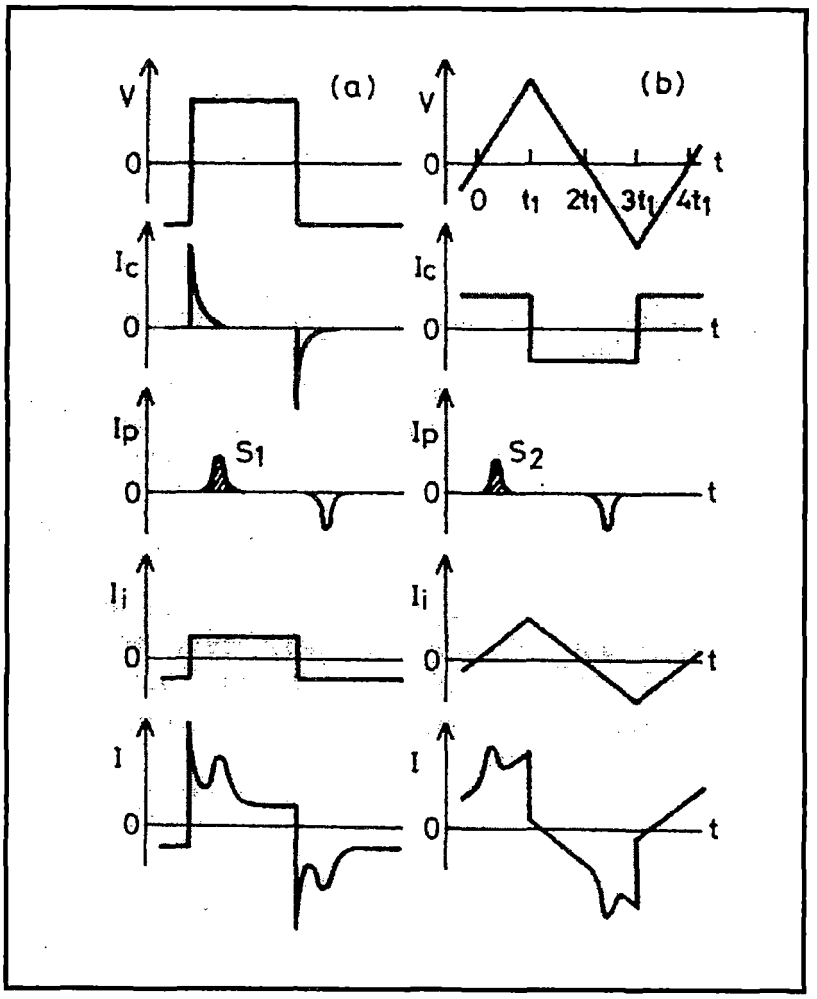

Figure 2.11. Schematic illustration of (a) the current induced by rapidly reversing a field and (b) by applying triangular voltage wave.

Spontaneous Polarization:

One of the most important physical quantities of FLCs is spontaneous polarization P_s. From the application point of view, the response time τ of ferroelectric switching is given by

$$\tau = \frac{\eta}{PsE} \qquad (2.68)$$

where η is a rotational viscosity of C- director on a cone and E is an applied electric field. The widely used three methods for determining P_s are (1) Sawyer-Tower method, (2) triangular method and (3) reverse field method. Some other methods that are also used are (4) electric-field dependent dielectric constant and (5) pyroelectric method. Here, the triangular method [134,135] is explained in comparison with the reverse field method.

Liquid crystalline compounds are not insulators. Hence, a liquid crystal cell can be regarded as a resistor 'R' and a capacitor 'C' connected in parallel. The current I(t) induced in a ferroelectric liquid crystal cell by applying a field V(t) is written as a sum of the following three contributions: (1) charge accumulation to the capacitor Ic, (2) the polarization realignment Ip and (3) ionic flow Ii.

$$I = Ic + Ip + Ii = C\left(\frac{dV}{dt}\right) + \frac{dP}{dt} + \frac{V}{R} \qquad (2.69)$$

where P is the amount of charge induced by the polarization realignment. P_s of FLCs is smaller than that of solid ferroelectrics by two or three orders of magnitude. This fact together with the higher conductivity of liquid crystals than that of the solid ferroelectrics make it difficult to measure P_s accurately.

Figure 2.11 illustrates the current induced by rapidly reversing a field or by applying a triangular voltage wave. The area S_1 or S_2 is equivalent to $2P_s$. It is clear that the current due to the polarization reversal is superposed on the exponential curve in the reverse field method and on a straight line in the triangular method.

Figure 2.12 shows an example of switching current signal in both methods. In these measurements, current signal was converted to voltage signal through a resistor of about 500 omhs, since P_s is relatively large. Hence, the time constant of

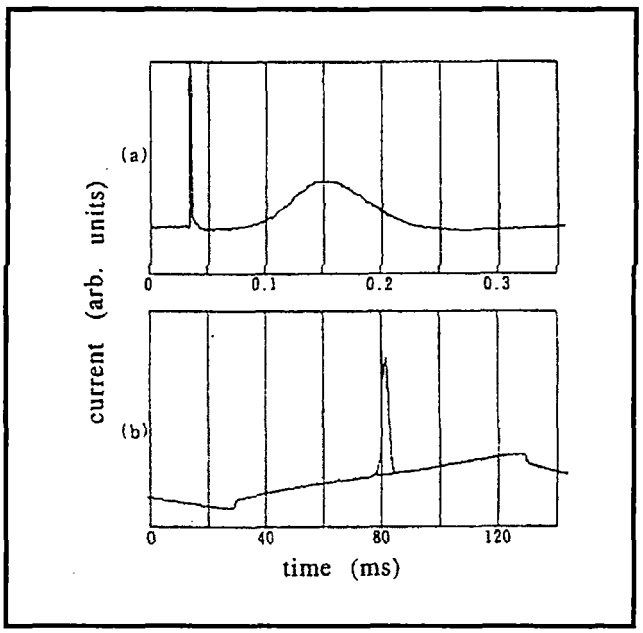

Figure 2.12. Switching current in (a) reverse field method and (b) the triangular method

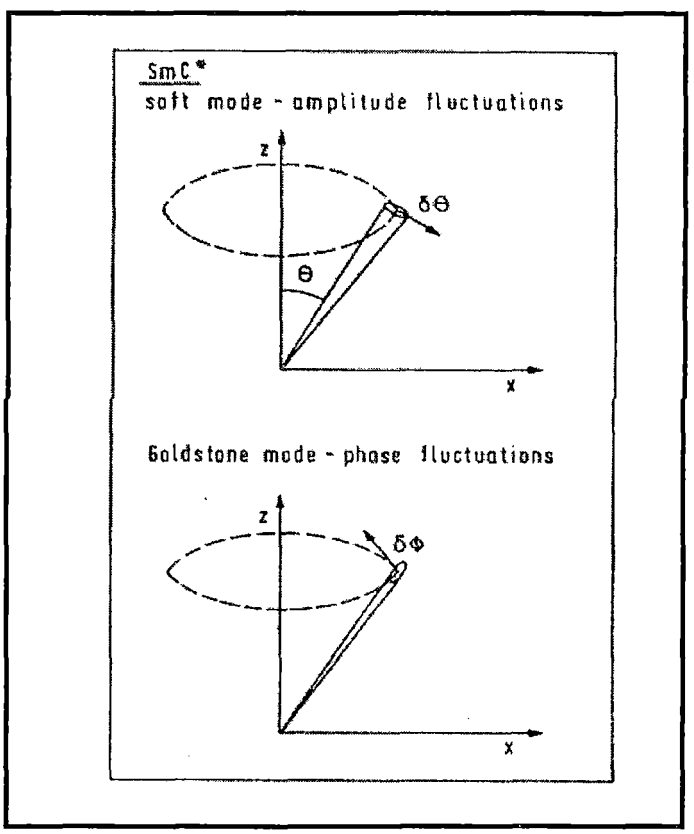

Figure 2.13. Soft mode and the Goldstone mode

the circuit is small, so that the current due to the charge accumulation is well resolved from the current peak due to the polarization reversal. When P_s is small and a large resistor or an amplifier must be used, Ip overlaps on Ic component in the reverse field method, which makes the separation of Ip component from the overall signal difficult. In the triangular method, however, the contribution of Ic and Ii appears as a straight line. In this respect, the subtraction of the base line is easier in the triangular method than in the reverse field method.

One has to be careful, when the material is relatively conductive and an applied electric field of low frequency is used in the triangular method. Ionic flow possibly gives rise to a current peak, which is sometimes reminiscent to the switching current peak.

Frequency domain dielectric spectroscopy (FDDS)

Debye model

One of the best ways to study dielectric behavior of a material consists in measuring of the complex dielectric permittivity versus frequency at constant temperature and ambient pressure. Dielectric studies under elevated pressure are also done for liquid crystals and FLCs [135]. Using FDDS in the case of polar liquid one obtains an absorption peaks in a certain frequency range, usually in the microwave region (1-100GHz). If one plots both the components of the dielectric permittivity on the logarithmic scale one obtain typical dielectric spectrum. Frequency dependence of ε' is known in the literature as the dispersion curve whereas that of ε'' is called the absorption curve.

The frequency at which ε'' reaches its maximum is known as critical frequency (or relaxation frequency). It can be described by the Debye-type formula:

$$\varepsilon^* = \varepsilon' - \varepsilon'' = \varepsilon_\infty + \frac{\varepsilon_0 - \varepsilon_\infty}{1 + i\omega\tau} \qquad (2.70)$$

where ε_0 is the static dielectric permittivity (known also as static dielectric constants), ε_∞ is the high frequency limit of the dielectric permittivity and τ is the dielectric relaxation time related to the critical frequency by the formula:

$$\tau = \frac{1}{2\pi\nu_c} \tag{2.71}$$

One should add that the Debye equation (2.70) could be split into two separate formulae:

$$\varepsilon' = \varepsilon_\infty + \frac{\varepsilon_0 - \varepsilon_\infty}{1+(\omega\tau)^2} \tag{2.72a}$$

$$\varepsilon'' = \frac{\varepsilon_0 - \varepsilon_\infty}{1+(\omega\tau)^2}\omega\tau \tag{2.72b}$$

where the first equation (2.72a) describes the dispersion and the second equation (2.72b) the absorption curve. ε'' reaches it's maximum at critical frequency:

$$\varepsilon''(\nu_c) = \varepsilon''_{max} = \frac{\varepsilon_0 - \varepsilon_\infty}{2} \tag{2.72c}$$

where the difference $\varepsilon_0 - \varepsilon_\infty \equiv \Delta\varepsilon_i$ is the so called dielectric increment that is also known in literature as dielectric strength.

Dielectric spectra is also presented by plotting ε'' versus ε' on the complex plain which is known as Cole-Cole plot or Cole-Cole diagram. Each point (ε', ε'') on the Cole-Cole plot represents complex dielectric permittivity obtained at a certain frequency. One should add that for the Debye-type process the Cole-Cole plot is a semicircle with the center lying on the ε' axis.

Cole-Cole model

Dielectric spectroscopy detects stochastic reorientation of molecular dipole moments and collective fluctuations of spontaneous polarization in paraelectric, ferroelectric, ferrielectric and antiferroelectric liquid crystals [136]. For liquids and solid rotator phases of organic polar compounds [137-139] the dielectric spectrum is usually of a Debye-type. However, some systems composed of flexible molecules

[138,140-142] and some disordered solid phases [143-145] exhibit broad dielectric spectra and can be described [138,143,146] by the Cole-Cole function:

$$\varepsilon^* = \varepsilon' - i\varepsilon'' = \varepsilon_\infty + \frac{\varepsilon_0 - \varepsilon_\infty}{1 + (i\omega\tau_0)^{1-\alpha}} - i\frac{\sigma}{\omega\varepsilon_0} \tag{2.73}$$

which can be separated into two component:

$$\varepsilon'(\omega) = \varepsilon_\infty + \Delta\varepsilon \frac{1 + (\omega\tau_0)^{1-\alpha} \sin\left(\frac{1}{2}\pi\alpha\right)}{1 + 2(\omega\tau_0)^{1-\alpha} \sin\left(\frac{1}{2}\pi\alpha\right) + (\omega\tau_0)^{2(1-\alpha)}} \tag{2.73a}$$

$$\varepsilon''(\omega) = \Delta\varepsilon \frac{1 + (\omega\tau_0)^{1-\alpha} \cos\left(\frac{1}{2}\pi\alpha\right)}{1 + 2(\omega\tau_0)^{1-\alpha} \sin\left(\frac{1}{2}\pi\alpha\right) + (\omega\tau_0)^{2(1-\alpha)}} + \frac{\sigma}{\omega\varepsilon_0} \tag{2.73b}$$

where $\Delta\varepsilon = \varepsilon_0 - \varepsilon_\infty$ is the dielectric strength, α is a parameter responsible for symmetric distribution of the relaxation times and τ_0 is in this case the most probable relaxation time related to the critical frequency ($\omega_0\tau_0=1$). $\varepsilon_0 = 8.85$ pFm^{-1} is the dielectric permittivity of the free space and σ is the conductivity of the studied substance. In (2.73) the conductivity term is added to classical Cole-Cole function. The maximum value of $\varepsilon''(\omega)$ depends on the parameter α according to the formula:

$$\varepsilon''(\omega_c) = \varepsilon''_{max} = \frac{\varepsilon_0 - \varepsilon_\infty}{2} \frac{\cos\frac{\pi\alpha}{2}}{1 + \sin\frac{\pi\alpha}{2}} \tag{2.74}$$

For small values of the α parameter ($\alpha < 0.1$) one can use the formula:

$$\varepsilon''_{max} \cong \frac{\varepsilon_0 - \varepsilon_\infty}{2 + \alpha\pi} \tag{2.74a}$$

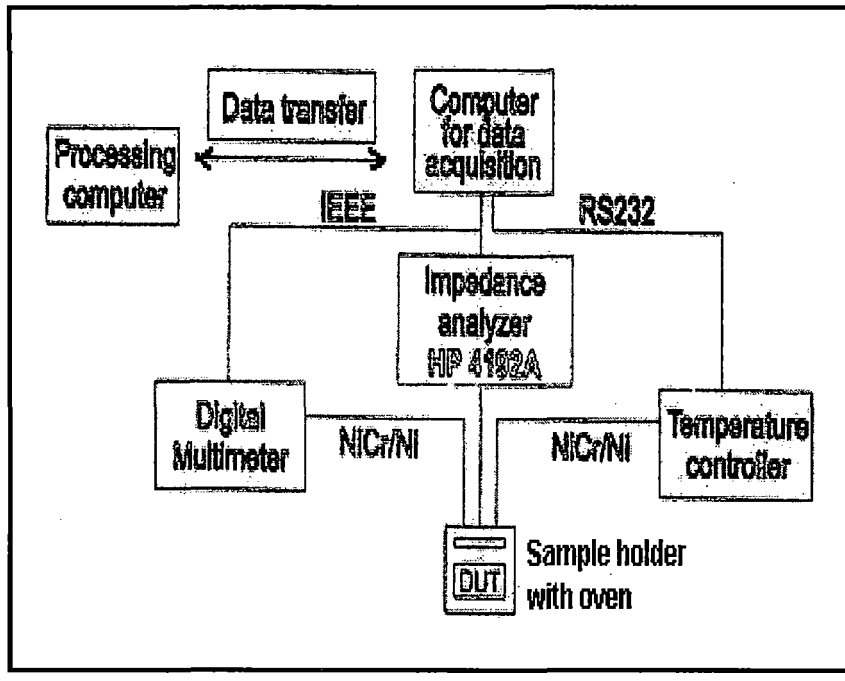

Figure 2.14. Schematic block diagram of the dielectric spectrometer.

so for non-Debye dielectric relaxation processes the absorption peak is lower and broader. A more general function [137,138] was proposed by Havriliak and Negami. Relaxation processes that could be described by this kind of function were observed for polymers, some disordered solids and also FLCs as well as AFLCs. Some of the dielectric relaxation processes observed in FLCs and AFLCs are pure Debye-type processes i.e. $\alpha=0$ and $\beta=1$ [147-153].

There are some other microscopic models proposed and used widely for data processing e.g. Cole-Davidson, Fuoss-Kirkwood [137,138], Jonscher [143,154] and so on.

Relaxation Modes

There exist several relaxation processes in FLC and AFLC: Goldstone mode, soft mode and rotation along molecular short and long axes, which appear in order of increasing frequency. The Goldstone mode (**Figure 2.13**) appears in the SmC^* phase because of the phase fluctuations in the azimuthal orientation of the molecular director and its characteristic frequency is usually less than 10 KHz. The soft mode, (**Figure 2.13**) on the other hand, appears in the neighbourhood of SmA^*- SmC^* transition due to fluctuations in the tilt angles of the molecules. Although hard to excite in comparison to the Goldstone mode, it softens near the transition point and this mechanism is usually observed at high frequencies. Both these modes are called collective mode since unlike molecular mode they represent collective behaviour of the molecules under the influence of the ac field. At still higher frequencies (~1GHz) absorption originates from stochastic reorientation of molecules around its axes. These are known as molecular modes.

Experimental Set Up

The experimental set up for the dielectric spectroscopy studies is shown in **Figure 2.14**. The computer controlled experimental apparatus consists of a HP4129A impedance analyzer and a Schlumberger Solatron 1250 FRA digital multimeter in conjuction with a self constructed amplifier based on the so-called

Chelsea Dielectric Interface principle [155]. A Eurotherm 818 controller allowed temperature control for the dielectric measurements from room temperature to 200^0C. The dielectric spectra were measured over the frequency range from 10 Hz to 10 MHz with 15 experimental points per decade.

References

1. E. B. Priestley, P. J. Wojtowicz and P. Sheng, Eds., *Introduction to Liquid Crystals*, Plenum Press, NY, (1974).
2. G. R. Luckhurst and G.W. Gray (Eds.), *The Molecular Physics of Liquid Crystals*, Academic Press, London(1979).
3. G. W. Gray and P. A. Winsor, Ed., *Liquid Crystals*, Vol.I and II, Ellis Horwood Limited (1974).
4. G. Vertogen and W. H. de Jeu, *Thermotropic liquid crystals: Fundamentals*, Springer – Verlag, Berlin (1988).
5. P. G. de Gennes, *The Physics of Liquid Crystals*, Clarendon Press, Oxford (1974).
6. W. Maier and A. Saupe, *Z. Naturforsch* **13a**, 564 (1958); *ibid.*, **14a**, 882 (1959); *ibid.*, **15a**, 287 (1960).
7. W. L. McMillan, *Phys. Rev.*, **A4**, 1238(1971).
8. W. L. McMillan, *Phys. Rev.*, **A6**, 936(1972). *ibid.*, **A8**, 1921 (1973).
9. M. Born, Sitzb. kgl. preuss, Ak. d. Wiss., phys. math. Klasse v. 25.5.1916, **XXX**, 614 (1916).
10. L. D. Landau and E. M. Lifshitz, *Ststistical Physics*, **Part I**, 3rd edn., Pergamon, Oxford (1980).
11. P.G. de Gennes, *Mol. Cryst. Liq. Cryst.*, 12,193 (1971).
12. K. K. Kobayashi, *J. Phys. Soc. (Japan)*, **29**, 101 (1970).
13. K. K. Kobayashi, *Mol. Cryst. Liq. Cryst.*, **13**,137 (1971).
14. A. L. Tsykalo, *Thermophysical Properties of Liquid Crystals*. Gordon and Breach Science Publishers, p 164, (1991).
15. R. B. Meyer and W. L. McMillan, *Phys. Rev. A*, **9**, 899(1974).
16. C. Zannoni in The Molecular Physics of Liquid Crystals, G. R. Luckhurst and G.W.Gray (Eds.), Academic Press, London(1979), Ch. 9.
17. C. Dasgupta in Liquid Crystals in the nineties and beyond, S. Kumar (Ed.), World Scientific, Singapore p 81, (1995).
18. R. Hasim, G. R. Luckhurst and S. Romano, *J. Chem. Soc. Farad. Trans.*, **91**(14), 2141(1995).
19. G. R. Luckhurst, S. Romano and H. B. Zewdie, , *J. Chem. Soc. Farad. Trans.*, **92**(10),1781(1996).
20. D. Frenkel in *Phase Transitions in Liquid Crystals*, S. Martellucci and A. N. Chester (Eds.), Plenum Press, NewYork (1992).
21. R. R. Netz and A. N. Berker, *Phys. Rev. Lett.*, **68**, 333(1992).
22. D. Frenkel and R. Eppenga, *Phys. Rev.*, **A31**, 1776(1985).
23. S. G. Dunn and T. C. Lubensky, *J. Phys. (Paris)*, **42**, 1201(1981).
24. A. L. Tsykalo, *Thermophysical Properties of Liquid Crystals*. Gordon and Breach Science Publishers, (1991).
25. P. J. Wojtowicz in E. B. Priestley, P. J. Wojtowicz and P. Sheng, Eds., *Introduction to Liquid Crystals*, Plenum Press, NY, p35 (1974).
26. R. L. Humphries, P. G. James and G. R. Luckhurst, *J. Chem. Soc., Faraday Trans. 2*, **68**, 1031(1972).
27. R. L. Humphries, P. G. James and G. R. Luckhurst, *Symp. Faraday Soc.*, no. **5**, 107, (1971).

28. P. Palffy-Muhoray, D. A. Dunmur, W. H. Muller and D. A. Balzarini, in *Liquid Crystals and Ordered Fluids*, Vol.**4**, ed. A. C. Griffin and J. F. Johnson, Plenum, NY, p. 615 (1984).

29. S. Chandrasekhar, *Liquid Crystals*, 2nd edn, Cambridge University Press, Cambridge, p51 (1992).

30. G. R. Luckhurst, *Quart. Rev.*, **22**, 179 (1968).

31. G. R. Luckhurst, *Mol. Cryst. Liq. Cryst.*, **21**, 125 (1973).

32. B. K. Vainstein, *Diffraction of X-rays by Chain Molecules*, Elsevier, Amsterdam, (1966).

33. A. J. Leadbetter in *The Molecular Physics of Liquid Crystals*, G.R. Luckhurst and G.W. Gray (Eds.), Academic Press, London, Ch. 14 (1979).

34. I. G. Chistyakov, *Sov. Phys. Usp.*, **9**, 551(1967).

35. L. V. Azaroff, *Mol. Cryst. Liq. Cryst.*, **60**, 73(1980).

36. J. Falgueirettes and P. Delord in *Liquid Crystals and Plastic Crystals*, G. W. Gray and P. A. Winsor(Eds.), Ellis Horwood(1974), **Vol. 2**, Ch. 3.

37. H. Kelkar and R. Hatz, *Handbook of Liquid Crystals*, Verlag Chemie(1980), Ch.5.

38. A. J. Leadbetter and E. K. Norris,. *Mol. Phys.*, **38**, 669(1979).

39. G. Ungar in *Physical properties of liquid* crystals, D. A. Dunmur, A. Fukuda and G. R. Luckhurst (Eds.),INSPEC, London(2001), Ch. 4.1

40. D. Demus and L. Richter, *Textures of Liquid Crystals*, Verlag Chemie, NY(1978).

41. A. J. Leadbetter and E. K. Norris, *Mol. Phys.*, **38**, 669(1979).

42. G. Vertogen and W.H.de Jeu (Eds.),*Thermotropic Liq. Cryst.Fundamentals*, Springer-Verlag. p-207(1988).

43. G. R. Luckhurst in *Liquid Crystals & Plastic Crystals* (Eds. G. W. Gray and P. A. Winsor), Ellis Horwood Limited(1974), Vol **2**, p-144.

44. C. L. Khetrapal and A. C. Kunwar in *Advances in Liquid Crystals* Vol. **1-6**, Ed. Glenn H. Brown, AP (1983). p-173.

45. V. D. Neff in *Liquid Crystals & Plastic Crystals* (Ed. G. W. Gray and P. A. Winsor), Ellis Horwood Limited(1974), Vol **2**, p-231.

46. S. J. Gupta, R. A. Gharde and A. R. Tripathi, , *Mol. Cryst. Liq. Cryst.*, **364**, 461 (2001).

47. B. Jha and R. Paul, *Proc. Nucl. Phys. and Solid State Phys. Symp., India* . **19C**, 491(1976).

48. B. Jha, S. Paul, R. Paul and P. Mandal, *Phase Transitions*, **15**, 39 (1989).

49. C. Kittle, *Intro to Solid State Physics*, Wiley Eastern, **Chapter 2** (1976).

50. A. J. Leadbetter and E. K. Norris, *Mol. Phys.*, **38**, 669 (1979).

51. B. Bhattacharjee, S. Paul and R. Paul, *Mol Phys.*, **44**, 139 (1981).

52. P. Mandal, R. Paul and S. Paul, *Mol. Cryst. Liq. Cryst.*, **131**, 299 (1985).

53. P. Sarkar, P. Mandal, S. Paul, R. Paul, R. Dabrowski and K. Czuprynski, *Mol. Cryst. Liq. Cryst.*, **330**, 159 (1999).

54. A. de Vries, *Mol. Cryst. Liq. Cryst.*, **10**, 219 (1970).

55. A. de Vries, *Mol. Cryst. Liq. Cryst.*, **11**, 261 (1970).

56. G. Pelzl in *Handbook of Liquid Crystals*. Vol. **1** (Fundamentals), Ed. D. Demus, J. Goodby, G. W. Gray, H.-W. Spiess and V. Vill, WILEY-VCH, Verlag GmbH, Weinheim, FRG 1998.

57. D. A. Dunmur in *The Optics of the Thermotropic Liquid Crystals*. Ed. S. Elston and R. Sambles, Taylor & Francis, 1998.

58. M. F. Vuks, *Optics and Spectroscopy*, **20**, 361, (1966).

59. H. E. J. Neugebauer, *Canad. J. Phys.* **32**, 1 (1954).

60. S. Chandrasekhar, *Liquid Crystals*, 2nd Edn., Cambridge University Press, Cambridge, p39, (1992).

61. W. H. de Jeu, *Physical Properties of Liquid Crystalline Materials*, Ed G. Gray, Gordon and Breach, Vol. **1**, p 41, (1980).

62. I. Haller, H. A. Huggins, H. R. Lilienthal and T. R. McGuire, *J. Phys. Chem.*, **77**, 950 (1973).

63. A. K. Zeminder, S. Paul and R. Paul, *Molecules. Cryst. Liq. Cryst.* **61**, 191 (1980).

64. K. Toriyama, K. Suzuki, T. Nakagomi, T. Ishibashi and K. Odawara, *J. de Phys*, **40**, C3-317 (1979).

65. S. Urban and H, Kresse in *Physical properties of liquid* crystals, (Eds. D. A. Dunmur, A. Fukuda and G. R. Luckhurst), INSPEC, London(2001), Ch 6.1 and 6.2

66. H. Kresse in *Handbook of Liquid Crystals*, Vols. **2A**, (Eds. D. Demus, J. Goodby, G.W. Gray, H.-W. Spiess and V. Vill, Wiley-VCH, Verlag GmbH, Weinheim, FRG (1998), p 91.

67. W. H. de Jeu and T. W. Lathouwers, *Z. Naturforsch* **29a**, 905 (1974).

68. *Theory of Electric Polarization*, Vol I (1973). 2nd edition Ed. C. J. F. Böttcher. and Vol II, 2nd edition Ed. C. J. F. Böttcher and P. Bordewijk. Elsevier Scientific Publishing Co. (1978).

69. D. A. Dunmur and W. H. Miller, *Mol. Cryst. Liq. Cryst.*, **60**, 281 (1980).

70. R. E. Michel and G. W. Smith, J. Appl. Phys. **45**, 3234(1974).

71. W. Maier and G. Meier, *Z. Naturforsch*, **16a**, 262 (1961).

72. L. Onsager, *Ann. N.Y. Acad. Sci.*, **51**, 627 (1949); *ibid, J. Am. Chem. Soc.*, **58**, 1486 (1936); *ibid, Phys. Rev.*, **62**, 558 (1942).

73. L. Bata and A. Buka, *Mol. Cryst. Liq. Cryst*, **63**, 307 (1981).

74. H. Frohlich, *Theory of Dielectrics*. Clarendon Press (Oxford, 1949); H. Frohlich, *J. Chem. Phys.*, **22**, 1804 (1954).

75. P. Bordewijk, *Physica*, **69**, 422 (1973).

76. P. Bordewijk, *Physica*, **75**, 146 (1974).

77. P. Bordewijk and W. H. de Jeu, *J. Chem. Phys.* **68(1)**, 116(1978).

78. W. H. de Jeu and P. Bordewijk, *J. Chem. Phys.* **68(1)**, 109(1978).

79. C. W. Oseen, *Arkiv Mat. Aston. Fysik*, **19**, 1 (1924), *ibid, Fortschr. Chem. Phys. Phys. Chem.* **20**, 1 (1929), *ibid, Trans. Faraday Soc.* **29**, 883 (1933).

80. H. Zocher, *Trans. Faraday Soc.* **29**, 945 (1933).

81. F. C. Frank, *Discuss. Faraday Soc.* **25**, 19 (1958).

82. J. Nehring and A. Saupe, *J. Chem. Phys.* **54**, 337 (1971).

83. F. Janhig and H. Schmidt, *Ann. Phys.* **71**, 129 (1972)

84. P. C. Martin, O. Parodi and P. S. Pershan, *Phy. Rev.*, A6, 2401 (1972).

85. M.G. Clark, *Mol. Cryst.Liq.Cryst.* **125**, 1(1985).

86. A. J. Leadbetter in *The Molecular Physics of Liquid Crystals*, G. R. Luckhurst and G.W. Gray (Eds.), Academic Press, London Ch. 13 (1979).

87. M. J. Bradshaw and E. P. Raynes, *Mol. Cryst. Liq. Cryst.*, **138**, 307 (1986).

88. H. Gruler and G. Meier, *Mol. Cryst. Liq. Cryst.*, **23**, 261 (1973).

89. Hp. Schad and M. A. Osman, *J. Chem. Phys.* **75**, 2 (1981).

90. N. V. Madhusudana and R. Pratibha, *Mol. Cryst. Liq. Cryst.*, **89**, 249 (1982).

91. M. F. Grebyonkin, G. A. Berenshev and V. V. Belyaev, *Mol. Cryst. Liq. Cryst.*, **103**, 1 (1983).

92. M. K. Das and R. Paul, *Mol. Cryst. Liq. Cryst.*, **250**, 13 (1994).

93. T. Moses and B. Jensen, Am. J. Phys., 66, 1 (1998).

94. W. H. de Jeu, *Physical Properties of Liquid Crystalline Materials*, Ed G. Gray, Gordon and Breach, Vol. **1**, p 17, (1980).

95. Structure. J. D. Bernal and D. Crowfoot, *Trans. Farad. Soc.*, **29**, 1032(1933).

96. P. Mandal and S. Paul, *Mol. Cryst. Liq. Cryst.*, **131**, 223 (1985).

97. P. Mandal, S. Paul, H. Schenk and K. Goubitz, *Mol. Cryst. Liq. Cryst.*, **135**, 35 (1986).

98. P. Mandal, B. Majumdar, S. Paul, H. Schenk and K. Goubitz, *Mol. Cryst. Liq. Cryst.*, **168**, 135 (1989).

99. P. Mandal, S. Paul, C. H. Stam and H. Schenk, *Mol. Cryst. Liq. Cryst.*, **180B**, 369 (1990).

100. S. Gupta, P. Mandal, S. Paul, M. de Wit, K. Goubitz and H. Schenk, *Mol. Cryst. Liq. Cryst.*, **195**, 149 (1991).

101. P. Mandal, S. Paul, H. Schenk and K. Goubitz, *Mol. Cryst. Liq. Cryst.*, **210**, 21(1992).

102. P. Mandal, S. Paul, K. Goubitz and H. Schenk, *Mol. Cryst. Liq. Cryst.*, **258**, 209(1995).

103. A. Nath, S. Gupta, P. Mandal, S. Paul and H. Schenk, *Liq. Crystals.*, **20**, 765(1996).

104. Pranab Sarkar, Parimal Sarkar, Pradip Mandal and T. Manisekaran, *Mol. Cryst. Liq. Cryst.*, **325**, 91(1998).

105. R. F. Bryan, Proceedings of the Pre-Congress Symposium on Organic Crystal Chemistry, Poznan, Poland, 105(1979); *J. Structural Chem.*, **23**, 128(1982).

106. W. Haase and M.A. Athanassopoulou, *Liquid Crystals*, D.M.P. Mingos(Ed.), Springer-Verlag, Vol. I, pp. 139-197 (1999).

107. A. J. Leadbetter and M. A. Mazid, *Mol. Cryst. Liq. Cryst.*, **65**, 265(1981).

108. B. K. Vainshtein, *Diffraction of X-rays by Chain Molecules*, Elsevier, Amsterdam, (1966), p12.

109. M. F. C. Ladd and R. A. Palmer, *"Theory and practice of Direct methods in Crystallography"*, Plenum Pub. Co., N. Y., (1980).

110. G. Germain, P. Main and M. M. Woolfson, *Acta Cryst.*, **B26**, 274 (1970).

111. H. Schenk and C. T. Kiers, *Simpel 83, an automatic direct method program package,* University of Amsterdam, 1983; H. Schenk, *Recl. Trav. Chim. Pays-bas,* **102**, 1(1983).

112. G. M. Sheldrick, *Direct method package program*, University of Gottingen, Germany (1993).

113. S. R. Hall and J. M. Stewart, *XTAL*, University of Western Australia and Maryland (1989).

114. A. Altomere, G. Cascarano, C. Giacovazzo, A. Guagliardi, M. C. Burla, G. Polidori and M. Camalli, *The SIR 92 Programme*, (1992).

115. P. S. White, *PC Version of NRCVAX (88)*, University of New Brunswick, Canada (1988).

116. Yao Jia-Xing, Zheng Chao-de, Quian Jin-Zi, Han Fu-Son, Gu Yuan-Zin and Fan Hai-Fu, *SAPI: A Computer Program for Automatic Solution of Crystal Structures from X-ary Data*, Institute of Physics, Academia Sinica, Beijing (1985).

117. C. J. Gilmore, *J. App. Cryst.*, **17**, 42 (1984).

118. C. J. Gilmore in *Direct Methods in Solving Crystal Structures*, H. Schenk (Ed), NATO ASI Series, Plenum Press, New York (1991), p177.

119. G. H. Stout and L. H. Jensen, *X-ray Structure Determination*, Macmillan, New York (1968).

120. M. J. Buerger, *Crystal Structure Analysis*, Wiley, New York (1960).

121. H. Schenk (Ed), *Direct Methods in Solving Crystal Structures*, NATO ASI Series, Plenum Press, New York (1991).

122. M. M. Woolfson, *An Introduction to X-ray Crystallography*, Cambridge University Press, London, (1970).

123. H. Hauptman and J. Karle, *Acta Cryst.*, **9**, 45 (1956); ibid., **12**, 93 (1959).

124. J. Karle and H. Hauptman, *Acta Cryst.*, **14**, 217 (1961).

125. J. Karle and I. L. Karle, *Acta Cryst.*, **21**, 849 (1966).

126. H. Schenk (Ed), *Direct Methods in Solving Crystal Structures*, NATO ASI Series, Plenum Press, New York (1991).

127. G. H. Stout and L. H. Jensen, *X-ray Structure Determination*, Macmillan, New York p195 (1968).

128. A. J. C. Wilson, Nature, **150**, 152(1942).

129. W. Cochran and M. M. Woolfson, *Acta Cryst.*, **8**, 1(1955).

130. W. Cochran, *Acta Cryst.*, **8**, 473 (1955).

131. J. Karle and H. Hauptman, *Acta Cryst.*, **9**, 635 (1956).

132. M. J. Buerger, *Crystal Structure Analysis*, Wiley, New York (1960).

133. G. H. Stout and L. H. Jensen, *X-ray Structure Determination*, Macmillan, New York(1968), p353.

134. FLC K. Miyasato, S. Abe, H. Takazoe, A. Fukuda and E. Kuze, *Jpn. J. Appl. Phys.*, **22**, L661 (1983).

135. Tutorials, *7th International Conference on Ferroelectric Liquid Crystals*, Darmstadt University of Technology, Germany (1999).

136. W. Haase and S. Wrobel, Eds., Dielectric Relaxation Spectroscopy, Springer-Verlag (2003).

137. C. J. F. Böttcher and P. Bordewijk, Ed., *Theory of Electric Polarization*, Vol II. Dielectric in time-dependent fields, Elsevier, Scientific Publishing Co. (1973).

138. N. Hill, W. E. Vaughan, A. H. Price and M. Davies, *Dielectric Properties and Molecular Behavior*, Van Nostrand, London (1969).

139. A. Wurflinger, *Int. Rev. Phys. Chem.*, **12**,89 (1993).

140. W.Haase, H. Pranoto, F. –J. Bormuth, *Ber. Bunsenges. Phys. Chem.*, **89**, 1229 (1985).

141. F. –J. Bormuth, Ph.D. Thesis, *Technische Hochschule*, Darmstadt (1998).

142. V. I. Minkin, O. A. Osipov, Y. A. Zhdanov, *Dipole Moments in Organic Chemistry*, New York-London, (1970).

143. A. K. Jonscher, Dielectric Relaxation In Solids, Chelsea Dielectric Press, London (1983).

144. S. Wrobel, B. T. Gowda, W. Haase, *J.Chem. Phys.*, **106**(10), 5904 (1997).

145. V. K. Agarwal and A. H. Price, *Mol. Cryst. Liq. Cryst.*, **98**, 193 (1983) and reference therein.

146. V. V. Daniel, *Dielectric Relaxation*, Academic Press, London and N.Y. (1967).

147. J. Hatano, Y. Hakanai, H. Furue, H. Uehara, S. Saito, and K. Murashiro, *Jpn. J. Appl. Phys.*, **33**, 5498 (1994).

148. S. Merino, M. R. de la Fuente, Y. Gonzalez, M. A. Perez Jubindo, M. B. Ros, J. A. Puertolas, *Phys. Rev.*, E**54**, 5169 (1996).

149. A. Fafara, B. Gestblom, S. Wrobel, R. Dabrowski, W. Drzewinski, D. Kilian, W. Haase, *Ferroelectrics*, **212**, 79 (1998).

150. M. Marzec, R. Dabrowski, A. Fafara, W. Haase, S. Wrobel, *Ferroelectrics*, **180**, 55 (1996).

151. H. Uehara, Y. Hakanai, J. Hatano, S. Saito and K. Murashiro, *Jpn. J. Appl. Phys.*, **34**, 5424 (1995).

152. M. Buivydas, S. T. Lagerwall, F. Gouda, R. Dubal, A. Takeichi, *Ferroelectrics*, **212**, 55 (1998).

153. H. Kresse, H. Schmalfuss, W. Weissflog, C. Tschierske, A. Hauser, *Mol. Cryst. Liq. Cryst.*, **366**, 505 (2001).

154. A. K. Jonscher, Limiting Losses in Dielectric. In IEEE *Transactions on Dielectrics and Electrical Insulation. Recent development in Dielectric and related Phenomena.* Eds. J. Ulanski, L. Okrasa, R. Gerhard- Multhaupt, G. Bak (IEEE Dielectrics and Electrical Insulation Society) Vol. **8**, No. 3, p 345 (2001).

155. D. Kilian, *Dissertation,* DUT, Darmstadt, (1999).